CALIFORNIA STATE UNIVERSITY, NORTHRIDGE

STRUCTURAL STYLE AND SHORTENING MAGNITUDE ACROSS OF THE KEPINTAGE FOLDAND THRUST BELT IN THE TIAN SHAN FORELAND, NORTHWEST CHINA

A thesis submitted in partial fulfillment of the requirements
for the degree of Master of Science
in Geology

By

Jozi Kerry del Angel

December 2012

The thesis of Jozi Kerry del Angel is approved:

_____	_____
J. Douglas Yule, Ph.D.	Date
_____	_____
Elena A. Miranda, Ph.D.	Date
_____	_____
Richard V. Heermance, Ph.D., Chair	Date

California State University, Northridge

DEDICATION

For my daughter, Zoie

ACKNOWLEDGEMENTS

It would not be possible for me to have finished this thesis without all the help, guidance, and support of many people. I would like to first thank my advisor, Dick Heermance. He has been an amazing mentor throughout graduate school. His ambition, guidance, and most of all, his confidence in me, has been critical in completing this thesis. I would also like to thank my committee members, Elena Miranda and Doug Yule, for providing constructive criticism on my thesis, and support throughout my graduate career. Special thanks also goes to my friends and colleagues in China, Chen Jie and his graduate students, for making it possible for me to complete my fieldwork in China. A thank you to Richard Allmendinger as well, he provided me with access to his trishear modeling program, as well as helpful tips through correspondence. I would also like to thank my close friends and family, especially my husband and daughter, for their endless support and putting up with me through late nights studying and weekends away on field trips. All of my fellow graduate students who travelled this journey with me also deserve thanks. I appreciate all the effort and encouragement from the rest of the CSUN geology faculty and staff. And last but not least, I would like to thank my kitties and my dog for all the late nights they kept me company.

PREFACE

This thesis is a stand-alone manuscript that utilizes data from a related project. All fieldwork completed in the field and referenced herein was conducted in the Summer of 2011 in conjunction with another Masters project. The associated project focused on sedimentology, paleoenvironment, and magnetostratigraphy, and is still in progress. This thesis utilized preliminary magnetostratigraphy completed as part of the associated project. A short section on magnetostratigraphy is included at the end of this manuscript as an appendix. All samples collected in the field for magnetostratigraphy were prepared for analysis in the California State University Northridge rock lab by Jozi Kerry del Angel. Samples were analyzed for Paleomagnetism at Occidental College in Los Angeles, California by Jeffrey Cook. All magnetostratigraphic correlations and analysis of the paleomagnetic data were completed by Dr. Richard Heermance.

TABLE OF CONTENTS

LIST OF FIGURES

LIST OF TABLES

ABSTRACT

STRUCTURAL STYLE AND SHORTENING MAGNITUDE ACROSS OF THE KEPINTAGE FOLD AND THRUST BELT IN THE TIAN SHAN FORELAND, NORTHWEST CHINA

By

Jozi Kerry del Angel

Master of Science in Geology

The Tian Shan represents intracontinental deformation related to the Indo-Asian collision, and thus provides an ideal location to study orogenic growth and the controls on foreland structural styles. The southern piedmont is dissected by faults and folds that vary in structural style along strike. Structural analysis, combined with magnetostratigraphy of Miocene and Pliocene sediments deformed in the foreland, provide data about the structural evolution of the mountain front. Mapping along the southernmost structure within the Kepintage thrust zone indicates the structure is a fault-propagation fold with a trishear component that has developed since the Pliocene. The gently dipping (25-35°) north limb contains ~8 km of Paleozoic and Cenozoic strata. The core of the anticline exposes intensely faulted Paleozoic strata. Total shortening across the structure, based on our cross section interpretation, is 10.5 +/- 1.1 km for a total shortening of approximately 33%. Preliminary magnetostratigraphy from Neogene strata on the northern flank of the fold indicate ages of deformed strata are ~14.5 - < 1.0 Ma, and growth strata at the top of the section are dated ~0.9 Ma. Growth strata provide maximum shortening rate estimates of 7.5 +/- 0.8 mm/yr. This rate is several times faster than the long-term geologic rates determined for this part of the foreland, but similar to short-term geodetically determined rates across the thrust belt at this location. Total shortening within the Kepintage thrust belt is ~35.3 +/- 3.5 km, which is more robust than several previous studies have indicated. However, our new observations suggest that over 35% of this shortening has occurred in only the last 2 million years, despite initial uplift of the range at approximately 20 Ma. Additionally, structural style appears to change from north to south. Fault-bend folds comprise the northern foreland and trishear fault-propagation folds the southern part. Furthermore, structural style varies along strike to the east and west of the study area. Contributing factors to controls on structural style are elucidated, including: thickness of Neogene strata, lithological variations, and location of décollement horizon. Our new interpretations suggest that shortening rates must have increased dramatically during the Quaternary at this location within the Tian Shan. Moreover, our data suggest that the Kepintage fault is a quite nascent feature, and illuminates the complex uplift history of the Tian Shan.

1. INTRODUCTION

Orogenic growth occurs through temporally and spatially complex deformation within the Earth's crust. In the case of convergent orogens, tectonic deformation is associated with crustal thickening, upward and outward growth of the mountain range, and the development of adjacent flexural basins within the foreland. These foreland basins in turn are uplifted and deformed as deformation migrates outward from the mountain range. Deformation rates within the foreland basins are directly related to growth of the orogen. In contrast, structural style may be controlled by the thickness and rheology of sediments, depth and geometry of the décollement, and/or presence of older, inherited structures (e.g., Butler et al., 2006, Lujan et al., 2003, Sepehr and Cosgrove, 2004, and Turner et al., 2010). Thus, integrated studies of shortening rates, structural style, and stratigraphy are imperative to determine the evolution of these mountain ranges.

Foreland basins display varying types of structural style that result from complex tectonic histories. These structural styles can be folds, faults, or a combination of both (e.g., McKnight, 1993, Yin et al., 1998, Allen et al., 1999, Hubert-Ferrari et al., 2006, Heermance et al., 2008, Regalla et al., 2010). If there is variability along strike, transfer zones, in the form of strike-slip or tear faults, may develop to accommodate the change (Turner et al., 2010). Alternatively, variations of structural style may be attributed to inherited structures (e.g. Butler et al., 2006, Iaffa et al., 2011). Shortening may be accommodated at different rates based on structural style, in other words, some styles may be able to accommodate faster rates than others. The root of why different structural styles exist along strike may provide insight into the long-term deformation of foreland basins and associated ranges. The deformation of the tectonically active foreland of the Tian Shan can be used as an analogue to understand ancient deformation of tectonically inactive mountain belts (Allen et al., 1999). Since hydrocarbon traps are often found in thrust belts similar to the forelands of the Tian Shan, an understanding of the structural variations may illuminate future hydrocarbon exploration and lateral compartmentalization of reservoirs (Turner et al., 2010).

In an effort to understand the causes of variable structural style along-strike in a foreland, this study will focus on the southern Tian Shan foreland basin in northwestern China (Figure 1). The Tian Shan foreland has the advantage of lateral juxtaposition of several different structural styles along its 2500 km-long active southern margin (e.g. Yin et al., 1998). The arid nature of this region, combined with recent uplift and deformation within the foreland, creates nearly total exposure of surface outcrops and structures, and allows us to compare variable foreland styles with observed shortening rates. Although some parts of the foreland have been extensively studied, geologic data are sparse for the Kepintage Thrust Belt (Kepintage belt) part of the foreland (Figures 2 & 3). Studies within the Kepintage belt have either focused on the Paleozoic strata (e.g., Turner et al., 2010) or are based on large-scale, reconnaissance-level structural studies (e.g., McKnight, 1993, Yin et al., 1998, Allen et al., 1999). In order to determine the relationships between stratigraphic thickness and structural style along the Tian Shan, this study focuses on the western portion of the Kepintage belt, where imbricate thrust faults expose Paleozoic strata that have been displaced above younger Neogene strata (Allen et

al., 1999) (Figure 4). In contrast to previous studies that look at the Kepintage belt as a genetically uniform belt (e.g., Yin et al., 1998, Allen et al., 1999), this study separates the Kepintage region into the western and eastern segments with distinct structural styles. The purpose of this paper is to determine the structural style and crustal shortening within the western Kepintage belt of the Tian Shan foreland. These results are compared with data from adjacent forelands to interpret the evolution of the entire rangefront. Preliminary magnetostratigraphy is used to determine the age of pre-tectonic Neogene strata deposited prior to deformation of the frontal structure within the fold-and-thrust belt. Additionally, structural measurements from the older structures to the north of the study focus area allow interpretations of the structural evolution of the foreland as deformation propagated away from the mountain front. This data, coupled with published geodetic data, provides new insight to the evolution of the Tian Shan foreland, India-Eurasia plate dynamics, and potential seismic hazards along the frontal structure of the western Kepintage belt, as well as improve our understanding of foreland basin deformation in general.

2. BACKGROUND

2.1 Study Area

The study area is located in northwestern China in the western Kepintage belt of the Kashi-Aksu thrust system of the Tian Shan foreland (Figures 1-3). The western Kepintage belt is located at ~76°45' to 77°45' east. There are three geomorphically distinct regions, these regions have been named for the Tashenkou drainage valley in the western Kepintage belt. The three regions are termed Southern Tashenkou region (the southern most region), Medial Tashenkou region (the middle region), and Northern Tashenkou region (the northern region) (Figure 5). The study area encompasses all three regions, but the focus of this study concentrates primarily on a linear transect that includes the Southern Tashenkou, Medial Tashenkou, and Northern Tashenkou regions, a cross strike map distance of approximately 60 km (Figure 3).

2.2 Tectonic History

2.2.1 Tian Shan

The Tian Shan (Shan means "mountain") extend approximately 2500 km from the Pamir ranges in the west to the China-Mongolia border in the east. Peaks in the Tian Shan exceed heights of 7000 m, making the Tian Shan the second tallest mountain range outside of the Himalayan orogen. The Tian Shan has been a topographic high (and therefore a source of sediment for the nearby basins such as the Tarim Basin) since the Paleozoic (e.g., Carrol et al, 1995 and Dumitru et al, 2001). Pre-Cenozoic history of the region now occupied by the Tian Shan is thought to include south vergent island arc collisions in the middle Paleozoic and again in the late Paleozoic and Mesozoic (e.g., Hendrix et al., 1992, Carroll et al., 1995), which collided with the northern edge of the passive margin of the Tarim Block (Allen et al., 1993). The present day growth of the Tian Shan, as well as the Himalaya, and many central Asian mountain ranges, are the result of continent-continent collision between India and Asia during the Cenozoic (e.g., Molnar and Tapponnier, 1975). It is curious that the Tian Shan are so far removed from the main part of the Himalaya. The Tian Shan is an ancient plate boundary (e.g., Molnar and Tapponnier, 1975); this ancient suture zone may have provided a belt of weakness in which deformation could propagate. Cenozoic uplift of the southern Tian Shan initiated between 21 and 24 Ma based on facies transitions of sediments in the Baicheng-Kuche Thrust System segment of the foreland (Figure 2) to the east of the Kepintage belt (Yin et al., 1998). Similarly, Sobel et al. (1997) uses apatite fission-track and suggest uplift initiation between 20-25 Ma along the Southern Tian Shan Fault, the southern bounding fault of the Tian Shan in the Kepintage region. Avouac et al. (1993) suggest that the Tian Shan were formed in the middle Miocene between 22-9 Ma and also suggest that central Asia experienced a "mid-Miocene crisis", or a change of regime in the Indo-Eurasia collision, that may have attributed to the rise of the Tian Shan. An alternative initiation of growth of the Tian Shan has been proposed by GPS (global positioning satellites) measurements. According to current geodetic data extrapolated to long-term geologic rates, the Tian Shan may have grown in only the past ~10 Ma (Abdrakhmatov et al.,

1996). This would rely on current shortening rates being steady over the past 10 Ma and has been suggested by some studies (e.g., Sun et al., 2004, Abdrokmatov et al., 2001).

2.2.2 Southern Tian Shan Foreland

The Tian Shan foreland has experienced at least three phases of deformation: middle Paleozoic, late Paleozoic to Mesozoic, and late Cenozoic (Yin et al., 1998). The late Cenozoic deformation is of particular interest in this study because it is associated with the Indo-Eurasian collision and deforms the southern foreland. Geodetic data can be used in conjunction with geologic shortening rates in the forelands to help determine long-term versus short-term shortening rates. Geodetic data provide shortening rates over the past couple decades, while geologic rates can tell us about shortening rates over the past several million years. Comparing long- and short-term rates can illustrate recent changes in rates of shortening along the foreland. Presumably, this southerly deformation in the Kepintage fold and thrust belt began in the late Cenozoic. Initiation of deformation of the foreland may, at the earliest, be coeval with Cenozoic growth of the Tian Shan. If geodetic rates were extrapolated backwards, it would suggest that the bulk of the growth of the Tian Shan has occurred over the last 10 Ma (Abdrokmatov et al., 1996). Turner et al. (2010), propose that deformation of the Kepintage fold and thrust commenced ~10-5 Ma, contemporaneous with the increase in growth of the Tian Shan in the late Miocene as suggested by Adbrokmatov et al. (1996). It can be assumed that deformation of the southern foreland did not begin prior to the growth of the Tian Shan, so an upper bounding age of 25 Ma (near the Oligocene-Miocene boundary) can be placed on the foreland deformation, and a lower bounding age of 10 Ma (Late Miocene). 10 Ma is used as the lower bounding age rather 5 Ma since it is a date in agreement between multiple authors (Turner et al., 2010 and Abdrokmatov et al., 1996). Also, as will be discussed later, an initiation at 5 Ma does not agree with correlations to adjacent foreland segments.

2.3 Regional Structural Geology

The Tian Shan foreland has along strike variation in sediment composition, thickness, structural style, and shortening rates. Yin et al. (1998) divide these variations into four segments from west to east, the Kashi-Aksu thrust system, the Baicheng-Kuche thrust system, the Korla transfer system, and the Lop Nor thrust system (Figure 2). Even within these segments variations exist. The southwestern edge of the Tian Shan foreland can be divided up into four sections that lie roughly between the cities of Kashi (Kashgar) and Aksu, collectively referred to as the Kashi-Aksu thrust system by Yin et al (1998) (Figure 3). The four sections of the Kashi-Aksu system, from west to east, are the Kashi Foreland Basin (~75°30’ - 76°45’ east), western Kepintage belt (~76°45’ - 77°45’ east), the eastern Kepintage (~77°45 - 79°20’ east), and the Aksu Re-entrant (~79°20’ - 80°30’ east) (Allen et al., 1999 and Turner et al., 2010) (Figure 3). Each segment of the Kashi-Aksu thrust system can be characterized by its structural style.

2.3.1 Kashi Foreland Basin

The westernmost segment of the Kashi-Aksu thrust system, the Kashi Foreland Basin, contains thick (~10 km) Neogene units stratigraphically above intensely deformed pre-Cenozoic strata. Cenozoic strata are deformed via detachment and wedge thrusts above a gypsiferous décollement horizon at the base of the Tertiary strata (Heermance et

al., 2008). The Kashi foreland consists of fault-bend folds in the northern part of the foreland, while detachments folds comprise the southern (more distal) parts (Heermance et al., 2008). Shortening rates across these structures have varied over the past 16.3 Ma; rates between 16.3 and 13.5 Ma were 1.1-3.2 mm/yr, between 13.5 and 4 Ma rates were <0.5 mm/yr, and since 4.0 Ma rates are estimated at 2.25-2.75 mm/yr (Heermance et al., 2008). These latter rates are much slower than the regional geodetic data of 8 +/-3 mm/yr (Abdrakhmatov et al., 1996 and Reigber et al., 2001) and 4-7 mm/yr (Zubovich et al., 2010) (Figure 6). Implying a temporal change in shortening rates.

2.3.2 Western and Eastern Kepintage

East of the Kashi foreland basin, the Kepintage belt is characterized by thin Neogene strata above an approximately >4 km thick Paleozoic sequence (e.g., Allen et al., 1999, McKnight, 1993, Yin et al., 1998). The Kepintage belt is approximately 200 km wide along strike and is distinguished from contiguous segments by its arcuate shape that pinches in toward the range front on either side (Figure 3). The Kepintage belt is bisected by a north-south trending sinistral tear fault (the Piqiang Fault), to the west of which Neogene strata are thickest (western Kepintage belt), to the east Neogene strata are less than 1000 m thick (eastern Kepintage belt) (e.g.: Allen et al., 1999). The structural style accommodating deformation of these strata have been characterized as thin-skinned thrusting associated with décollement in a Cambrian evaporite horizon (e.g.: Turner et al., 2010 and Allen et al., 1999). The structural style of the Kepintage belt has been described as having a ramp-flat geometry, or fault-bend folding, detaching in an Upper Cambrian sedimentary horizon (McKnight, 1993), fault-propagation folding with a similar décollement horizon (Allen et al., 1999), as well as deformation through imbricate thrust faulting in the eastern Kepintage (Turner et al., 2010). Turner et al. (2010) does not specifically divide the Kepintage into the western and eastern segments, but recognized several distinct differences across the Piqiang Fault. All other studies typically consider the area as one segment. Few detailed mapping studies in the Kepintage belt have been completed to provide field support for either of these interpretations. Despite this structure not being exposed, several workers have estimated various depths for the décollement of the western Kepintage belt. Estimates of the depth to décollement at 6-7 km have been made through crude calculations from Chinese maps and cross sections (McKnight, 1993). Depths to detachment of 5.5-9 km and 6 km were used by Allen et al. (1999) and Turner et al. (2010), respectively. It is presumed that the décollement horizon is the same for all structures within the western (and eastern) Kepintage belt. The décollement horizon is thought to lie within a weak sedimentary horizon in the Cambrian strata (e.g., McKnight, 1993, Turner et al., 2010, Allen et al., 1999).

2.3.3 Aksu Re-entrant

To the east of the eastern Kepintage belt, structural style again changes to a thick-skinned thrust zone (Allen et al., 1999). The Aksu Re-entrant is composed of a low angle thrust fault and detachment folds (Hubert-Ferrari et al., 2005). The area of deformation also varies along the mountain front; the whole Kepintage fold and thrust belt is a relatively thick zone of deformation compared to the Aksu Re-entrant where a significant amount of deformation is confined to the Aksu Thrust at the foot of the Tian Shan (Hubert-Ferrari et al., 2005). Only two structures accommodate significant shortening in this region, the Aksu thrust fault and the Aksu Anticline (Figure 3). The Aksu thrust fault

is the southern bounding fault of the Tian Shan in the Aksu Re-entrant, it has a shallow dip of approximately 10°-20° (Hubert-Ferrari et al., 2005). The Aksu Anticline and the Aksu thrust fault have a décollement surface at the base of the Cenozoic strata (Hubert-Ferrari et al., 2005). Shortening across these structures over the past 12,500 years is estimated to be 6.5 mm/yr, which is consistent, within error, with geodetic data of 8 +/- 3 mm/yr (Hubert-Ferrari et al., 2005). It is curious to note that the peaks of the Tian Shan above the Aksu Re-Entrant are the highest peaks of the range (Jengish Chokusu at 7439 m above sea level). Not to say that this implies faster shortening rates than elsewhere in the foreland, rather that much of the shortening in this region may be accommodated by the mountain front thrust. The Kuche fold and thrust belt (Figure 2) has been interpreted as having two structural styles, detachment folding and complex fault-bend folding. Shortening rates over the last 600,000 years is estimated to be 4-5 mm/yr, based on the kinematic modeling method of Epard and Groshong (1995) (Hubert-Ferrari et al., 2006). These rates are also slower than the regional geodetic data of 8 +/- 3 mm/yr (Reigber et al., 2001) and 4-7 mm/yr (Zubovich et al., 2010); this may indicate an increase in rate over time (Hubert-Ferrari et al., 2006).

2.3.4 Fault-Propagation Folds versus Fault-bend Folds

The structural style of the Kepintage fold and thrust belt has consistently been described as all fault-bend folds (McKnight, 1993, Yin et al., 1998) or all fault-propagation folds (Allen et al., 1999), with little consideration into the possibility of alternative structural styles or combinations of structural styles. As a hanging wall fault block rides over a ramp in the fault plane, the hanging wall fault block will bend; this is known as a fault-bend fold (Suppe, 1983). Fault-bend folds have a ramp-flat geometry where slip is uniformly distributed along the fault surface, and the hanging wall and footwall do not exhibit overturning (Figure 7). Kink-band modeling can be used to model Fault-bend folds with out the use of a computer program.

Another type of fold that can form above a fault is a fault-propagation fold. According to Suppe (1983), fault-propagation folds exhibit compression in front of a fault tip during deformation (Figure 7). They are asymmetrical folds that develop in front of a propagating fault (Cristallini and Allmendinger, 2002). Slip on the fault surface decreases up dip in a fault-propagation fold and they often have an overturned forelimb.

2.4 Shortening Rates

Previously published geodetic data are not consistent with estimated long-term geologic shortening rates in all areas of central Asia (e.g.: Heermance et al., 2007 and Hubert-Ferrari et al., 2006) (Figure 6). This may be reconciled by temporal changes in rates of shortening across various structures of the forelands. Geodetic data for the region are tabulated below in Table 1. Geodetic rates are much faster than estimated long-term geologic rates. Yin et al. (1998) and Allen et al. (1999) proposed long-term geologic shortening rates of 1-1.9 mm/yr and 1.8 mm/yr in the region, respectfully.

Table 1 - Shortening Rates Relative to the Stable Kazakh Platform

Region	Rate
India into Asia	40-50 mm/yr[2], 45 mm/yr[3]
Across the Tian Shan	20 mm/yr[1,3], 20 +/-2 mm/yr[4]
Across the Himalaya	20 mm/yr[2]
Across the Kunlun	10 mm/yr[2]
Across the Kashi-Aksu Thrust Belt	8 +/-3 mm/yr[2]
Tarim Basin beneath the Tian Shan (foreland)	4-7 mm/yr[4]

Geodetic data from [1]Abdrakhmatov et al., 1996, [2]Reigber et al., 2001, [3]Yang et al., 2008, and [4]Zubovich 2010.

3. METHODS

3.1 Field Work

3.1.1 General Field Work

Field mapping was conducted over 14 days in June 2011. Strike and dip measurements were taken along a 16 km traverse between the Southern Tashenkou region and the Medial Tashenkou region (Figures 3-5). Additionally, strike and dip measurements were taken in select locations throughout the broader study area encompassing regions to the north of the Medial Tashenkou (Figure 5). Locations of all strike and dip locations were plotted on Google Earth images of the area. As no foreigners are permitted to have topographic maps or GPS units in China, all field mapping was done on high-resolution Google Earth images. Locations of faults and significant changes in lithology were recorded on the images. Additionally, photos, sketches, and notes were used to record observations in the field.

3.1.2 Stratigraphy of the Western Kepintage foreland

The stratigraphy in the western Kepintage is composed of approximately 3800 m of Tertiary strata and 4300 m of Paleozoic strata. The 4300-meter thick Paleozoic section of the stratigraphic column was compiled from previously published literature and fieldwork, such as basic field observations and strikes and dip measurements. The Tertiary section of the stratigraphic column was created by measuring the stratigraphy with a Jacob staff and describing the lithology in the field. Approximately 3800 meters of Tertiary strata were measured with a 1.5 meter Jacob staff equipped with an Abney level.

Age control of the Tertiary strata are constrained through magnetostratigraphy and correlation with Kashi basin strata to the west. Samples were collected for magnetostratigraphy by fellow graduate student Jeff Cook and this work is ongoing. A brief overview of the magnetostratigraphy is included as an appendix to this thesis (Appendix B & C). Age controls for the Paleozoic strata are based on previously published literature (McKnight, 1993). The thicknesses of the Neogene strata were measured in the field and used to create the cross section. Thicknesses of the Paleozoic strata determined based on surface dip data and Google Earth imagery, and correlated with previously published data, were used to create the cross section.

3.2 Structural Analysis

3.2.1 Structure and Shortening

Structural analysis included collecting strike and dip measurements on sedimentary bedding features and fault zones, as well as trend and plunge of slickenlines. Each field measurement was carefully labeled on Google Earth imagery. These data were incorporated into the geologic map (Figure 5) and cross sections completed in the program "FaultFoldForward" from Dr. R. Allmendinger at Cornell University. This program creates balanced cross sections based on dip data of the fault plane, or dip data of strata above the fault plane. A topographic profile with dip data, fault locations, stratigraphic contacts, and depth to décollement was drafted (Figure 8). This topographic profile was then superimposed on the cross section iterations in FaultFoldForward to find a best-fit match. The best fit The comprehensive balanced cross section through the field

area allowed interpretation of total shortening magnitude across each structure by using the slip on the fault planes in conjunction with an area balanced and restored cross section. This method appears similar to the line-length method in that it follows both a pre- and post-deformation horizon. It compares the pre- and post-deformation length from just above the décollement horizon across the section. It differs in that each successively higher stratigraphic layer will produce less shortening magnitudes due to thickening and thinning of strata during deformation. In shear deformation, the difference in shortening between the uppermost-deformed strata and the lowermost-deformed strata can vary significantly (e.g., Marshak and Nicolas, 1998, and Suppe et al., 2004). Therefore, only the strata just above the décollement horizon can be used to estimate shortening magnitudes. Length of shortening is determined by the equation:

$$\Delta l = |l_{final} - l_{initial}|$$

where Δl is the change in length, l_{final} is post-deformation length, and $l_{initial}$ is pre-deformation length

Shortening percentage (e) is determined by the equation:

$$e = ((l_{final} - l_{initial}) / l_{initial}) \times 100$$

where e is the percent change in length (a negative number indicates shortening, while a positive number would indicate extension)

The line length method requires a pin line on either side of the structure, ideally with strata at a pin line horizontal, or undeformed. Conventionally, a pin-line is drawn straight and perpendicular to bedding in a deformed cross section (Marshak and Nicholas, 1998). This pin-line must be either, straight and perpendicular to strata, or a loose line that smoothly varies in the restored cross section (Marshak and Nicholas, 1998). The value for $l_{initial}$ is determined by using a marker bed; the length of the marker bed is measured through the deformed strata between the two pin lines. Pin-lines on either side of the deformed cross section must adhere to specific rules that are dictated by conservation of mass and geometric relationships. A restored cross section can then be drawn to provide support that the deformed cross section is balanced, as well as visually illustrate the amount of shortening. The value for l_{final} is determined by measuring the linear distance between the two pin lines. The assumption is made that a negligible amount of material moves in or out of the cross section line parallel to thrust motion. Four stratigraphic layers were used to determine the shortening. As stated above, only the layer immediately above the décollement horizon provides reliable shortening magnitudes.

3.2.2 Rates of Shortening

Shortening magnitude was combined with the youngest ages of deformed strata in order to quantify shortening rates across the foreland. The shortening rates of the Southern Tashenkou structure can be determined by using the following equation:

$$\textbf{Rate} = \Delta \textbf{l}/\textbf{Time}$$

Shortening rates determined herein are all geologic rates and can be compared to previously published geodetic rates (gedetic fig, Table 1).

4. RESULTS

4.1 Stratigraphy

4.1.1 Paleozoic Stratigraphy

There is up to 4300 m of Paleozoic strata exposed in the western Kepintage (Figure 9). The oldest strata consist of Cambrian to Ordovician age limestone from the décollement horizon to approximately 2000 m above the décollement. Above the Ordovician limestone is ~1500 m of Middle Silurian to Devonian age red and green siltstones and sandstones. Next is ~500 m of fossiliferous limestone, followed by ~100 m of oolitic limestone, then ~200 m of interbedded siltstones and sandstones all of which are Carboniferous in age. The boundary between the Neogene and Paleozoic strata are an unconformity characterized by a basal breccia. All Paleozoic ages are from previously published studies (e.g., McKnight, 1993, Allen et al., 1999, and Turner et al., 2010). An evaporite horizon, possibly salt or gypsum, is believed to exist within the Cambrian limestone, providing the weak layer that deformation has exploited as the décollement layer (e.g., McKnight, 1993, Turner et al., 2010, Allen et al., 1999).

4.1.2 Tertiary Stratigraphy

The measured Tertiary strata (Figure 9) are approximately 3800 m thick and composed of mudstones, siltstones, sandstones, and conglomerates. This section is capped by the time transgressive Xiyu Conglomerate (e.g., Heermance et al., 2007, Charreau et al., 2009).

The stratigraphy of the Tertiary strata can be subdivided into 4 fundamental units. The lower unit is from 0 to 665 meters and is composed of mudstones, siltstone, and a distinctive green shale. Overlying the lower unit are ~1400 m of sandstone. The sandstone section is from 665 to 2082 meters in the stratigraphic column and is composed of thick sandstone beds with large-scale cross-beds and thin shale units separating each succession. These strata pinch out towards the west into strata of the lower unit. The next unit is from 2082 to 3380 meters and is composed of interbedded shale and siltstone, this unit grades into a conglomerate section from 3380 to 3500 meters. The uppermost 300 m (~3500-3800 meters) consist of 0.5-1 m-thick conglomerate beds.

4.2 Structure

4.2.1 General structural style of the western Kepintage belt

4.2.1.1 Structural style of the Northern Tashenkou region

The region most proximal to the mountain front, or northern part of the foreland, has been subject to a significant amount of erosion and there is little topographic relief associated with this structure (Figure 4 & 5). Only a handful of strike and dip measurements were collected in this region. Initially, the deformation evident here appeared to be a single distinct structure and has been mapped and interpreted as such (McKnight 1993). Regardless of the limited amount of dip data for this region, it became evident that the Northern Tashenkou region is comprised of two structures, one of which is buried (Figure 10). Surface dip data in this region are steep, up to 60°-70°, but change to 30° towards the south (Figure 11). This can be explained by stacking two structures on top of one another, one fault surface is translated over a subsequent fault surface thus

doubling the dip data on the surface. Changes in dips moving south, from 60°-70° to 30°, and no evidence of overturned strata suggests that the two structures are fault-bend folds (Figure 10). In addition to the surface dip data implicating the presence of a buried structure, immediately to the east of the Piqiang fault the buried structure emerges.

4.2.1.2 Structural style of the Medial Tashenkou region

The next region to the south of the Northern Tashenkou region is the Medial Tashenkou region (Figure 4, 5, & 10). It is constrained to a greater extent, with more than 30 strike and dip measurements collected in this region (several measurements were from several km to the west of the cross section and have been projected parallel to strike). It was immediately evident that the structural style of the Medial Tashenkou region is different from the Northern Tashenkou region. Near the North Kepintage Thrust Fault there were thinned strata and overturned strata in the hanging wall. Additionally, shear deformation was evident as 1 m-thick gouge zones, brecciated fault cores, and shear fabrics (Figure 12). The Medial Tashenkou region was identified as being composed of a single south verging fault-propagation fold.

4.2.1.3 Structural style of the Southern Tashenkou region

The southernmost part of the study area is called the Southern Tashenkou region (Figure 4, 5, & 10). This region is very well constrained by hundreds of strike and dip measurements. The area between the Kepintage Thrust Fault and the North Kepintage Thrust Fault is where the 3800 meters of Neogene strata were measured. The Southern Tashenkou region has many of the same characteristics as the Medial Tashenkou region, with shear deformation, overturned strata, and thinned strata near the Kepintage Thrust Fault (Figure 13). In addition to these observations, there was a change in dip of the bedding between the faults. To the south, the dips are shallow, 10^{o}-20^{o}, moving north the dips increase to 30^{o} -40^{o}, and most proximal to the North Kepintage Thrust Fault the dips increase to over 60^{o} (Figure 14). This region is also identified as being composed of a south verging fault-propagation fold.

4.2.1.4 Structural style modified

Complications arose while hand drafting the cross section for the Southern Tashenkou and Medial Tashenkou regions. The dip data, unit thicknesses, and known points of contact between different units proved problematic for reconciling the subsurface geometries of both structures using the same depth to detachment. It was evident that both of these structures were fault-propagation folds, as both exhibited shallowly dipping back limbs and steep to overturned forelimbs, an asymmetrical geometry, and faulting at the surface. However, using the kink band model to produce a comprehensive cross section through these two structures would not allow me to maintain a single décollement horizon. Moreover, the substantial amount of shear in the forelimb of both structures indicated that there may be a significant shear component present that may affect the interpretation of the structural style. I explored alternative interpretations of these two structures and found that a trishear model of fault-propagation folding fit the field data well. Trishear modeling, however, must be done iteratively through numeric modeling, and cannot be hand rendered. Refer to Appendix D for details on trishear.

4.2.2 Modeling the structural styles

4.2.2.1 Southern Tashenkou and Medial Tashenkou Regions – Fault-propagation folding with a trishear component

Within the cross sectional area, the fault zone for the Southern Tashenkou and Medial Tashenkou regions can be seen at the surface. In the Southern Tashenkou region, the Kepintage Thrust Fault is exposed in a wide shear zone, and there is not a discrete fault plane evident. In the Medial Tashenkou region, the North Kepintage Thrust Fault is exposed as a brittle shear zone with shear structures, discrete fault planes, and fault gauge (Figure 12).

The fundamental problem encountered using a kink-band model for the structures within the Southern Tashenkou and Medial Tashenkou regions was abiding by the surface dip data and contacts, while preserving the same depth to décollement for both structures. There is no indication that depth to décollement would change between these two structures. The Paleozoic strata are of similar thickness, and the structures in the Northern Tashenkou region should conform to the same décollement horizon as the Southern Tashenkou region. The exposed strata near the fault zones of the Southern Tashenkou and Medial Tahsonkou region thin, or tighten, as described in trishear modeling. In exploring trishear modeling for cross section construction, I superimposed the model runs over a cross sectional profile of the study area that included points of contact of different units, dip measurements, and locations of faults to create a comprehensive cross section (Figure 8). The values that created the best fit for the structures identified in the Southern Tashenkou and Medial Tashenkou regions are shown in Table 2.

There appears to exist an additional structure burgeoning in the subsurface beneath the prevalent structure in the Southern Tashenkou region. The surface dip data are fairly consistent in the backlimb, moving northward away from the axial surface of the structure. The strata dip approximately 10-20° to the north for approximately 8 km, then the dip increase to approximately 30°-40° for 3 km, then increase to >60° for the remaining 2 km (Figure 14). This increase in dip can be resolved by either folding of the northern limb or by the formation of a new structure in the subsurface. The steeper dips to the north, however, are incompatible with any models of south-vergent trishear folding, and thus we interpret a second structure must be present in the subsurface. This nascent structure has little slip on the fault surface as evident by the small amount of surface expression seen in the surface dip data. To incorporate the budding structure, I used trishear criteria similar to that of the structure in the Southern Tashenkou region, with a total slip value of 4.0 km.

Table 2 – Trishear Values for structures in the Medial Tashenkou and Southern Tashenkou Regions

Data	Medial Tashenkou	Southern Tashenkou visible structure	Southern Tashenkou blind structure
Ramp angle	30°	20°	20°
Trishear angle	60°	60°	60°
P/S ratio:	1.2	0.8	0.8
Total slip (km)	13.8	14.5	4.0

4.2.2.2 Northern Tashenkou – fault-bend fold duplex

The Northern Tashenkou structure has been identified as a duplex structure based on two main criteria: 1) dip data on the back limb of the exposed structure that can be reconciled by the presence of an additional ramp in the subsurface, and 2) to the east of the Piqiang fault, two structures are evident at the surface. Moreover, the surface dip data will not allow the subsurface to be resolved with a fault-propagation structure, and there is no evidence of an asymmetrical structure, or overturned forelimbs, as is the case with the Southern Tashenkou and Medial Tashenkou structures (Figure 10).

A duplex structure can be modeled using the kink-band method; however, to model a cross section across all structures with a single model makes for a more fluid assessment of the interaction of all structures. Therefore, I used the trishear model to model all structures. By setting the P/S ratio = 1 and the trishear angle to zero for the two structures, the influence of the trishear component is minimized. Unfortunately, both the backlimb and forelimb cannot be controlled to behave similarly to kink-band modeling. By controlling the backlimb and allowing for a minor shear component in the front limb, the model better fits the surface observations. If the stratigraphy becomes more shaly, and thus more ductile, to the south, this would be reasonable. The forelimb will behave according to a trishear model, some shear will be induced in the model; however, this is not a problem when attempting to determine shortening, only for determining the geometry of the material in the forelimb, which in this study has mostly been eroded away. Based on surface dip data and stratigraphic contacts, the values used to model the structures in the Northern Tashenkou region are in Table 3.

Table 3 – Trishear Values for Structures in the Northern Tashenkou Region

Data	Northern Tashenkou – Exposed Structure	Northern Tashenkou – Buried Structure
Ramp angle	30°	30°
Trishear angle	0°	0°
P/S ratio:	1	1
Total slip (km)	7.5	4.0

4.2.2.3 Best-fit cross section model

Multiple iterations were completed before a best-fit cross section was revealed. The iteration included in this document fit the dip data and the locations of contacts and faults best. Figure 15 illustrates the difference in the structural style demonstrated in this study compared to previous studies. This is the first study to identify more than one structural style normal to strike in the western Kepintage belt.

4.2.4 Comprehensive structural style and change north to south

There exists a distinct change in the structural style as deformation moved away from the mountain front. The structural style of the western Kepintage has evolved as deformation propagated away from the mountain front. An initial structural style of fault-bend folding dominated, and changes to a trishear style fault-propagation folding towards the south.

According to critical wedge theory, deformation progrades from the mountain front to the foreland (e.g., Davis, 1983, Dahlen et al., 1990). This is evident in the western Kepintage, where the structures are more proximal to the mountain front are not as well preserved as the more distal structures. Moreover, preliminary magnetostratigraphy (Appendix B & C) and correlation of structures in the western Kepintage to dated structures in the Kashi Basin support temporal progradation of deformation basinward. In total there exist five structures in the western Kepintage; the oldest two, the Northern Tashenkou duplex structure, exhibit a fault-bend fold geometry, and the progressively younger Medial Tashenkou and Southern Tashenkou structures of a trishear fault-propagation style, as well as the nascent structure below the Southern Tashenkou fault. A comprehensive balanced cross section reveals the geometric integrity of these styles (Figure 10).

4.3 Timing

4.3.1 Growth strata

Growth Strata were observed at the top of the Xiyu Conglomerate on the back limb of the Southern Tashenkou structure (Figure 16). Initially we believed that the growth strata provided us with a constraint on the timing of the initiation of deformation of the Southern Tashenkou structure. Growth strata are formed when deposition is syntectonic. As a structure grows, and sedimentation continues, a characteristic thinning of strata toward the structure will be produced (Riba, 1976; Suppe et al., 1997). In other words, growth strata can be described as strata that are deposited on a deforming surface creating a characteristic upward fanning of the newly deposited strata. Growth strata are coevally deposited with growth folding (Verges et al., 2002). Based on the preliminary magnetostratigraphic results, the base of the growth strata are ~0.9 Ma, indicating active deformation. However, as a structure grows, growth strata can be buried, exposed, or eroded (Verges et al., 2002). The growth strata observed on the hanging wall of the Southern Tashenkou structure are exposed. It was unclear as to whether or not older growth strata lower in the section have been eroded away. It is possible that as growth strata were deposited, the hanging wall of the Southern Tashenkou structure was translated over subsurface faulting and folding, thus bringing the newly deposited strata over the same structures and eroding growth strata during deformation. Therefore, the extrapolated age of the growth strata of 0.9 Ma is not used as timing of initiation in this

study, rather it is noted and its presence is expressed as a structure that has been syntectonically deposited. Also, since the age of the growth strata are extrapolated, the actual age of the strata may differ. The age of 0.9 Ma at the base of the growth strata (above the Xiyu Conglomerate) is important because the Medial Tashenkou structure cuts these growth strata and reveals that this structure was active during the Quaternary.

4.3.2 Structure correlation and age constraint

Correlation of structures in the western Kepintage belt to the structures in the Kashi basin provide the best age constraint of structure growth since structures appear to be genetically related to one another along strike (Figure 17). Structural lineaments can be traced from the western Kepintage belt into the Kashi Basin. The Atushi Anticline can be correlated to the structural lineament of the Southern Tashenkou region and the Keketamu Anticline can be correlated to the structural lineament of the Medial Tashenkou region. Initiation of deformation of the Atushi and Keketamu Formations are constrained at ~1.4 Ma and ~4 Ma, respectively (Heermance et al., 2008). These ages are consistent with preliminary magnetostratigraphy and cross-cutting relationships of the structures within the Southern Tashenkou and Medial Tashenkou regions. Our new data imply that structures were active at 0.9 Ma. Timing of deformation within the Medial Tashenkou and Southern Tashenkou regions can be constrained between 4-0.9 Ma, and 1.4-0.9 Ma, respectively.

4.4 Shortening

4.4.1 Timing constraint within the western Kepintage belt

The cross section across the western Kepintage includes five structures for which total shortening is estimated (Figure 10). Shortening rates are also estimated for the main structure and burgeoning structure in the Southern Tashenkou (C-C') region, the single structure in the Medial Tashenkou (B-B') region, as well as cumulative shortening rates across the entire foreland basin (A-A'). Age constraint for A-A' is based on initial uplift of the Tian Shan at 25-10 Ma (Avouac et al.,1993, Sobel et al., 1997, Yin et al., 1998, Abdrokmatov et al., 2001, Sun et al., 2004). Age constraint for B-B' and C-C' is determined by correlation of the structural lineaments in the western Kepintage belt to the previously published dates of structures in the Kashi Basin.

4.4.2 Total shortening and potential shortening rates across the western Kepintage belt

Total pre- and post-deformation lengths were measured normal to strike across the western Kepintage belt (Figure 10). The marker beds, or contacts used in determining the pre-deformation length are the top of the Neogene, the Neogene-Paleozoic contact, the Ordovician-Silurian contact, and the décollement surface. These stratigraphic layers were used because they are continuous and easy to follow throughout the section. Total shortening magnitudes are presented in Table 4.

Table 4 – Shortening Magnitudes

Cross Section Location	Stratigraphic Interval	$l_{initial}$	l_{final}	Δl
Western Kepintage A-A'	Top of Neogene	81.4 km	60 km	-21.4 +/- 2.1 km
	Neogene-Paleozoic contact	81.4 km	53.3 km	-28.1 +/- 2.8 km
	Ordovician-Silurian contact (Lm-Clastic contact)	81.4 km	48.8 km	-32.6 +/- 3.3 km
	Above décollement surface	**81.4 km**	**46.1 km**	**-35.3 +/- 3.5 km**
Medial Tashenkou section B-B'	Top of Neogene	24 km	15.4 km	-8.6 +/- 0.9 km
	Neogene-Paleozoic contact	24 km	13.9 km	-10.1 +/- 1.0 km
	Ordovician-Silurian contact (Lm-Clastic contact)	24 km	12.2 km	-11.8 +/- 1.2 km
	Above décollement surface	**24 km**	**11.1 km**	**-12.9 +/- 1.3 km**
Southern Tashenkou section C-C'	Top of Neogene	31.5 km	31.1 km	-0.4 +/- 0.04 km
	Neogene-Paleozoic contact	31.5 km	25.9 km	-5.6 +/- 0.6 km
	Ordovician-Silurian contact (Lm-Clastic contact)	31.5 km	22.9 km	-8.6 +/- 0.7 km
	Above décollement surface	**31.5 km**	**21 km**	**-10.5 +/- 1.1 km**

Décollement surface represent approximate shortening magnitudes, other horizons presented to illustrate change in shortening magnitudes. Error is arbitrarily assigned at 10%.

A range of shortening values are produced, this is due to the effect of the trishear component. Beds may thin and/or thicken in trishear modeling making it difficult to determine shortening magnitudes using the traditional line length method. They are presented in Table 3 to illustrate that the cross section can be area balanced, but cannot be used to determine shortening with the line-length method. Therefore, the shortening magnitude used in this study is based of the strata at the top of the décollement, or fault, surface since this horizon has a finite value that was input into the FFF program to create the model. It has the least amount of shear associated with it since it is a discrete fault. Other studies have also used fault surfaces, or dip slip horizons to estimate magnitudes of shortening (e.g., Regalla et al., 2010). Total shortening magnitude on the surface between A-A' is 35.3 +/- 3.5 km (Table 4). This is calculated using the pre- and post-deformation length of the strata just above the décollement horizon.

4.4.3 Total shortening across the Southern Tahenkou and Medial Tashenkou

Total shortening between B-B' is 12.9 +/- 1.3 km, or 49-59%. This is approximately 37% of the total shortening of the foreland. Total shortening between C-C' is 10.5 +/- 1.1 km, or 30-36%. This is approximately 30% of the total shortening of the foreland. This implies that at least 65% of the shortening in the western Kepintage occurred in the structures in the Medial Tashenkou and Southern Tashenkou region

4.4.4 Shortening rates across the western Kepintage belt

If it is assumed that all the deformation of the foreland is confined to the structures defined herein and that growth of the Tian Shan pre-date, or is at least coeval with the deformation of the foreland, the total shortening determined above and the age of the growth of the Tian Shan can be used to quantify shortening rates. Using the max age of 25 Ma can provide the absolute minimum shortening rates of the western Kepintage. Using the timing of foreland folding and thrusting as suggested by Turner et al. (2010) will provide that absolute maximum shortening rates. This age can be used to estimate maximum shortening rate estimates across the whole western Kepintage. Table 5 illustrates the minimum, maximum, and preferred rates of shortening.

4.4.5 Shortening rates across the Southern Tashenkou and Medial Tashenkou regions

Shortening rates for the Southern Tashenkou and Medial Tashenkou are estimated with the amount shortening, or change in length, as determined above. The minimum age for thrust initiation is constrained by growth strata appearing at that time and cross-cutting relationships. It is evident that both structures were active 0.9 Ma. Growth strata on the backlimb of the Southern Tashenkou, with an estimated date of 0.9 Ma indicate that the structure was growing at that time. The Medial Tashenkou structure exhibits thrusting over the same growth strata. The maximum age for thrust initiation is constrained by correlation of structures to the Kashi Basin (Figure 17). Shortening values, age constraints, and shortening rates are presented in Table 5.

Table 5 – Shortening Rates

Location		Shortening Magnitude	Min age	Max age	Min rate	Max rate
Western Kepintage A-A'	Age and Rate range	35.3 +/- 3.5 km	10 Ma	25 Ma	1.4 +/- 0.1 mm/yr	3.5 +/-0.4 mm/yr
	Preferred age and rate:		20 Ma		**1.8 +/- 0.2 mm/yr**	
Medial Tashenkou B-B'	Age and Rate range	12.9 +/- 1.3 km	0.9 Ma	4 Ma	3.2 +/- 0.3 mm/yr	14.3 +/- 1.4 mm/yr
	Preferred age and rate:		4 Ma		**3.2 +/- 0.3 mm/yr**	
Southern Tashenkou C-C'	Age and Rate range	10.5 +/- 1.1 km	0.9 Ma	1.4 Ma	7.5 +/- 0.8 mm/yr	11.7 +/- 1.2 mm/yr
	Preferred age and rate:		1.4 Ma		**7.5 +/- 0.8 mm/yr**	

Note that 10 Ma is used instead of 5 Ma for the minimum initiation of deformation for the Western Kepintage, this is because of the structure age of the Medial Tashenkou is determined to be ~ 4 Ma through correlation to the Kashi Basin (Figure 17), an initiation of deformation of only 1 My earlier would imply an unreasonably high rate of shortening for the structures older than this in the foreland. Preferred age of structure based on ages used for shortening estimates determined by Allen et al. (1999) and Yin et al. (1998). Error is arbitrarily assigned at 10%.

5. DISCUSSION

5.1 Neogene strata interpretation

The Tertiary strata can be subdivided into four units. These units can be correlated along strike to the west in the Kashi Basin and can be correlated to the Wuqia Group, the Atushi Formation, and the Xiyu Conglomerate. The lower unit is 0-665 meters and is composed of mudstones, siltstone, and a distinctive green shale. These strata can be interpreted as mudflats, and meandering fluvial and overbank deposits and correlate laterally with the Wuqia Group to the west (Heermance et al., 2007). Overlying the lower unit are ~1400 m of sandstone. This sandstone section is located at 665 to 2082 meters in the stratigraphic column and is composed of thick sandstone beds with large-scale cross-beds and thin shale units separating each succession, it can be interpreted as aeolian. These strata pinch out towards the west into strata of the lower section and correlates as a member of the Wuqia Group. The next unit is located at 2082 to 3380 meters and is composed of interbedded shale and siltstone, which correlate laterally with the Atushi Formation (Heermance et al., 2007). These strata are interpreted as overbank fluvial and floodplain deposits, similar to the Atushi Formation to the west (Heermance et al., 2007). (Heermance et al., 2007). The next unit grades into the Xiyu Conglomerate from 3380 to 3500 meters. The uppermost 300 m (~3500-3800 meters) consist of 0.5-1 m-thick conglomerate beds interpreted as braided stream deposits; this is the Xiyu Conglomerate (Heermance et al., 2007).

The ages of the Wuqia Group and Atushi Formation have been suggested by other workers as Miocene (Bally et al., 1986, Heermance et al., 2007) and Pliocene (Yin et al., 2002, Heermance et al., 2007) in age, respectively. Within the Kashi Basin the ages of the Wuqia Group and Atushi Formation are 18-5.3 Ma and 5.3-0 Ma, respectively (Heermance et al., 2007). The Xiyu formation is time transgressive from 15.5 +/- 0.5 Ma to 1.9 +/- 0.2 Ma (Heermance et al., 2007).

According to preliminary magnetostratigraphy from Jeff Cock's thesis work (Appendix B & C), the lower Neogene unit (the Wuqia Group) in the western Kepintage is ~14 to 12.5 Ma, the aeolian section is 12.5-6.8 Ma, the uppermost Neogene unit (the Atushi Formation) is 6.0-1.6 Ma, and the Xiyu Conglomerate is 1.6-0.9 Ma (Figure 9, Appendix C - Figure A3 & A4). Thus, the western Kepintage strata are Miocene to Pliocene in age.

5.2 Variations in Neogene and Paleozoic Stratigraphic Thickness

The Paleozoic strata have been described as being of similar thickness throughout the Kepintage fold and thrust belt (McKnight, 1993). However, others have described the Paleozoic strata as thickening towards the north within the foreland (Carroll et al., 1995 and Yin et al., 1998). The observation that thrust imbricates are regularly spaced at an interval of 12 km – 15 km, each with the same décollement horizon, implies that the Paleozoic strata are of equal thickness throughout the western and eastern Kepintage fold and thrust belt (Yin et al., 1998). This study shows how the Neogene strata vary from ~10 km in the Kashi Basin, to 3800 m in the western Kepintage area, to <2000 m to the east of the Piqiang fault. Moreover, the thickness of the Neogene strata increases away from the mountain front within the Kepintage. This change in thickness is evident by the

Paleozoic strata exposed in the backlimbs of the structures in the Medial Tashenkou region and the Southern Tashenkou region. At its thickest, the Neogene strata are approximately 3800 m based on measured section between the Southern Tashenkou and Medial Tashenkou regions. North of the Medial Tashenkou region, the Neogene strata thin to approximately 2000-2500 m based on thickness calculations from dip data and satellite imagery. This implies that deformation of the foreland began within the Neogene. Uplift and erosion of Neogene strata cut off sedimentation in the north while syntectonic deposition continued south of the active structures. In other words, as structures grew in the Neogene, their unroofed sediments were deposited on the pre-deformation surface to the south, which was subsequently deformed.

To the west of the Kepintage, in the Kashi foreland basin, there exists >6 km of Tertiary strata and up to 1000 m of Cretaceous strata and 1400-3800 m of coal-bearing Jurassic sediments (Carroll et al., 1995). In the western Kepintage, up to 4 km of Tertiary strata exist (with thinner strata to the north), and no Mesozoic strata (e.g., this study, McKnight, 1993, Turner et al., 2010). In the eastern Kepintage, the Tertiary strata are thinner and eventually pinch out to the west of Aksu city (e.g., Hubert-Ferrari et al., 2005 and Allen et al., 1999). East of Aksu city, in the Aksu Re-entrant, combined Tertiary and Mesozoic strata are 6-7 km thick (Hubert-Ferrari et al., 2005). This is a drastic variability in post-Paleozoic strata thickness.

5.3 Pre-existing Structures

Paleogeography and inherited structures may contribute to the variation of thicknesses of post-Paleozoic strata (Figure 18). The Kepintage fold and thrust belt contains several north-south striking strike-slip tear faults, the thickness of Paleozoic sediments across these faults change abruptly (Turner et al., 2010). Several strike-slip faults were present before deposition of any Cenozoic strata within the western and eastern Kepintage fold and thrust belt in western China (Turner et al., 2010). These faults control the thickness of Cenozoic strata, which in turn contribute to controls on the style of subsequent deformation. A major fault that illustrates this abrupt change is the Piqiang Fault, a fault that evidently cuts through Neogene strata and deformation (Figure 5). There is a net loss of ~800 m of Paleozoic sediment to the east of the Piqiang fault (Turner et al., 2010). The combination of the Piqiang fault cutting Neogene strata and deformation, with the change in Paleozoic strata thickness across it, implies that this fault is a pre-existing feature that has either been reactivated, or has been continuously active since the before the Neogene. Additional strike-slip faulting may be responsible for compartmentalization of segments within the Kashi-Aksu thrust system.

5.4 Controls on Structural Style: Variability in the Foreland

5.4.1 Variation in Post-Paleozoic Strata

It is evident that the structural style changes along strike throughout the Kashi-Aksu thrust belt. West to east, the style changes from detachment and wedge-style thrusts, including fault-bend folds (Heermance et al., 2007), to fault-bend folding and fault-propagation folding with a trishear component (this study), to imbricate thrust faulting (Turner et al., 2010), to a main shallow dipping thrust fault and detachment fold (Hubert-Ferrari et al., 2005) (Figure 3). These structures are all accommodating

shortening within the same foreland, the Kashi-Aksu thrust belt, yet there are differing structural behaviors amongst contiguous regions within the foreland. The main difference in these regions is thickness of post-Paleozoic strata (e.g., Yang et al., 2002, Hubert-Ferarri et al., 2005, Heermance et al., 2007) (Figure 19). The lithological variations, or presence of varying thicknesses of younger strata, may be causal to the variation in structural style. The Kashi basin and Aksu Re-entrant segments of the Kashi-Aksu thrust belt have relatively thick post-Paleozoic strata with deformation confined to the Cenozoic strata with décollement in a thick evaporite horizon (e.g.: Hubert-Ferrari et al., 2005, Heermance et al., 2007, and Scharer et al., 2004). Furthermore, there is little variation in depth of evaporite horizons along strike within the foreland (e.g., Scharer et al., 2004, Hubert-Ferarri et al., 2005, Heermance et al., 2007) (Figure 19). The décollement horizon will exploit the weakest units in the subsurface. If the lithology in which the décollement horizon lies varies, the impact to structural style may be significant. The thickness of the strata and the lithology above the décollement may dictate the structural style that prevails. In each segment of the Kashi-Aksu thrust belt, structural style (e.g. detachment folding, fault-bend folding, fault-propagation folding) is correlated with the thickness and composition of Cenozoic strata.

5.4.2 Variations within each segment of the Kashi-Aksu thrust belt

5.4.2.1 Kashi foreland basin

In the Kashi foreland basin, where the Tertiary strata are up to 10 km thick, detachment folding is the dominant structural style. Moreover, the décollement surface is near the base of the Tertiary strata within thick gypsiferous horizons, and does not incorporate the Paleozoic strata (Scharer et al., 2004 and Heermance et al., 2007). Likewise, the wedge thrust faulting, identified more proximal to the Tian Shan, detaches near the base of the Tertiary. Basement thrusts are most proximal to the range front (Heermance et al., 2008). The foreland evolves basinward to fault-bend folding (Tashipishake Anticline), then detachment folding (Atushi and Kashi Anticlines) with detachment at the base of the Tertiary (Heermance et al., 2008).

5.4.2.2 Aksu Re-entrant

Structural style in the Aksu Re-Entrant to the east is distinctly different, as observed in the number of structures that accommodate shortening, and in aerial view. Hubert-Ferrari et al. (2005) points out that the Mesozoic and Tertiary strata disappear to the west of Aksu city (until the Tertiary strata re-appear near the Piqiang Fault). Similar to structures in the Kashi basin, the Aksu Anticline detaches at the base of the Cenozoic (Hubert-Ferrari et al., 2005). The absence of post-Paleozoic stratigraphy in the Aksu Re-Entrant act as a mechanical barrier for deformation accommodation (Hubert-Ferrari et al., 2005). Accommodation of deformation in the Aksu Re-entrant appears to oscillate between the range front thrust and the Aksu Anticline (Hubert-Ferrari et al., 2005). This may in part be due to changes in stress fields (Hubert-Ferrari et al., 2005). In the Aksu Re-entrant, post-Paleozoic strata are all but absent; this may make it easier for the range front thrust to accommodate more of the deformation.

5.4.2.3 Western Kepintage belt

The western Kepintage belt exhibits a change in structural style as deformation has moved away from the mountain front. Tertiary strata here are ~4 km thick. The older

structures, in the Northern Tashenkou region, are fault-bend folds, and Tertiary strata here are thinner and are estimated to be ~2-2.5 km thick. Therein lies the observed correlation between the decrease in thickness of Cenozoic strata, coupled with change in structural style. These observations can be extrapolated to along-strike variations; changes normal to strike are also observed in adjacent segments. In the Kashi Basin a change from fault-bend folds to detachment folds exists, as well as stratigraphic thickness basinward (Heermance et al., 2007).

5.4.2.4 Implications from Post-Paleozoic Strata Thickness

The presence of thick evaporite horizons near the base of the Cenozoic strata in the Kashi foreland basin and Aksu Re-Entrant have provided a means for the development of detachment folds that involve only the Cenozoic strata (e.g., Hubert-Ferarri et al., 2005, Heermance et al., 2007, and Scharer et al., 2004). The Cenozoic strata are appreciably thinner in the Kepintage fold and thrust belt compared to the Kashi foreland basin and the Aksu Re-Entrant. At its thickest (~4 km thick), the Neogene strata are approximately 40% thinner than the contiguous forelands. Young soft sediments, like those found in the Cenozoic strata in this region (sandstones and siltstones), may not be suited for fault-propagation folding. Fault-propagation folds are not observed in the segments with thick soft sediment pile (the Kashi Basin), or very thin to no soft sediment pile (Aksu Re-entrant). This implies that the thickness of soft sediments is a controlling component of structural style. Similarly to the western Kepintage belt, structural style in both the Aksu Re-Entrant and the Kashi foreland basin vary from the north to south within each respective foreland.

Unfortunately, in the region where the Neogene strata disappear, to the west of Aksu city, the structural style is not well defined, therefore no congruent comparison can be made. The only region where fault-propagation folding is identified is within the Kepintage fold and thrust belt, where relatively thin Neogene strata overly Paleozoic strata. Also, a nontrivial point is the presence of fault-bend folds within the western Kepintage, which is a structural style recognized elsewhere within the foreland. Fault-bend folding is present in regions where the post-Paleozoic strata are relatively thick (up to 10 km); as in the Kashi foreland basin (Heermance et al., 2007 and Scharer et al. 2004) (Figure 19 & 20). Paleozoic strata are found in the cores of anticlines in the Kashi Basin (Heermance et al., 2008), however, the western and eastern Kepintage belt are the only regions within the Kashi-Aksu thrust system that incorporates a significant amount of Paleozoic strata in the deformation. Décollement occurs in the Cambrian limestone, ~4 km beneath the Neogene-Paleozoic contact, rather than at the base of the young Neogene strata. Décollement is approximately 6-10 km below the surface in the Kashi foreland basin (Scharer et al., 2004, Heermance et al., 2008) and 7-8 km below the surface in the Aksu-Re-Entrant (Yin et al., 1998), and ~8 km beneath the surface in the western Kepintage at the southern margin and ~6 km beneath the surface further north where fault-bend folding is dominant, a fairly similar detachment depth (Figure 20). Moreover, the décollement horizon lies within an evaporite horizon for all three sections (e.g., McKnight, 1993, Allen et al., 1999, Hubert-Ferrari et al., 2005, Heermance et al., 2007, and Scharer et al., 2004).

5.4.2.5 Implications from Paleozoic Strata Thickness

The Paleozoic Limestone units are cliff-forming strata within the western Kepintage belt (Figure 21). Thickness of the Paleozoic strata may imply that folding instability prompted the development of thrusts (Yin et al., 1998) rather than folds. It is possible that the lithology of the Paleozoic strata may contribute to this folding instability. The décollement horizon is thought to lie within an evaporite layer in limestone, roughly 2 km below the Cambrian-Ordovician contact (McKnight, 1993, Yin et al., 1998, Allen et al., 1999, and Turner et al., 2010). There is ~2 km of limestone directly over the décollement horizon, as well as an additional 600 m of limestone beginning ~3.5 km above the décollement. In the Kashi foreland basin, <40 m of limestone strata are present anywhere above the décollement (Heermance et al., 2007). In the Aksu Re-Entrant there is a lack of detailed stratigraphic descriptions; however, since the northern passive margin of the Tarim craton was destroyed near the end of the Late Permian (Allen et al., 1993), and growth of the Tian Shan began in the Middle Miocene (Avouac et al., 1993), the likelihood of appreciably thick limestone units in the Mesozoic or Cenozoic strata are doubtful. Due to the presence of thick limestone strata that lie above the décollement horizon in the western Kepintage, the lithology may have had a significant impact on the formation of fault-propagation folds over fault-bend folds and detachment folds. It may be easier for a fault to propagate to the surface in the old, hard limestone of the western Kepintage and easier to only slide on décollement horizons in young, softer rocks as in the Kashi foreland.

5.3 Shortening

5.3.1 Geologic Shortening

Previous studies have indicated a total minimum shortening within the Kepintage fold and thrust belt at 50 km (McKnight, 1993), 23 km (Yin et al., 1998), and 35 km (Allen et al., 1999). Allen et al., (1999) assumes an initiation of deformation at approximately 20 Ma for the foreland, arriving at a shortening rate of ~1.8 mm/yr. In this study, I determine an amount shortening for the whole foreland of 35.3 +/- 3.5 km. This is similar to what Allen et al. (1999) determined. If the initiation of deformation of the whole foreland is 20 Ma, using the amount of shortening determined herein of 35.3 +/- 3.5 km, a rate of shorting of 1.8 +/- 0.2 mm/yr is calculated. This rate is similar to rates determined by Allen et al. (1999) and Yin et al. (1998) of 1.8 mm/yr and 1-1.9 mm/yr, respectively. Table 4 illustrates the range of shortening rates possible for the western Kepintage, 0.9-4.4 mm/yr

Across the Medial Tashenkou region and the nascent Southern Tashenkou region, shortening rates are determined to be approximately 3.2 +/- 0.3 mm/yr km, and 7.5 +/- 0.8 mm/yr, respectively (Table 7). The shortening rates of the foreland increases from 1.8 +/- 0.2 mm/yr to 3.2 +/- 0.3 mm/yr to 7.5 +/- 0.8 mm/yr implying a long term increase in shortening rates within the Kepintage, or at least variation in rate over time.

5.3.2 Geologic vs. Geodetic Shortening Rates

The geologic shortening rate determined herein for the Southern Tashenkou region of 7.5 +/- 0.8 mm/yr is comparable to the current geodetic data of 8 +/- 3 mm/yr (Reigber et al., 2001) and 4-7 mm/yr (Zubovich et al., 2010) (Figure 6), yet significantly faster than the long-term shortening estimated herein for the whole western Kepintage

belt (1.8 +/- 0.2 mm/yr). Geodesy provides current, short-term shortening rates, while geologic shortening rates are long-term. Since these rates are a different scale, caution should be expressed in comparing the two rates. Nonetheless, this infers that the structures in the Southern Tashenkou region are much more active than previously thought, and further supports an overall increase in shortening rates over time.

Stratigraphic thickness of the Neogene strata on the backlimb of the exposed structure in the Northern Tashenkou region is much thinner than that of the backlimb of the structure in the Medial Tashenkou region. As structures grew in the Northern Tashenkou region, sediment was supplied to the south, implying that the structures in the Northern Tashenkou region were active before the Medial Tashenkou. This same reasoning can be applied to the Medial Tashenkou region being active prior to the Southern Tashenkou region, therefore, deformation propagated south. If the structures in the Northern Tashenkou region are definitively the first structure to be active in the western Kepintage belt, the Northern Tashenkou region was active at ~20 Ma to as recently as ~ 4 Ma (when the Medial Tashenkou region was first active). Deformation was then taken over by the Medial Tashenkou region at 4 Ma, and by the Southern Tashenkou region at 1.4 Ma. Overthrusting of Paleozoic strata over growth strata on the backlimb of the main structure in the Southern Tashenkou region indicate that the Medial Tashenkou region was active at 0.9 Ma, temporally overlapping with deformation in the Southern Tashenkou region. These same growth strata indicate that the Southern Tashenkou region was active at 0.9 Ma, possibly even more recently. Geologic shortening rates across each region imply an overall increase in shortening overtime. Additionally, shortening rates across the Southern Tashenkou region are similar to current geodetic data.

6. CONCLUSIONS

New mapping of the western Kepintage has identified five structures. The structures most proximal to the mountain front are fault-bend folds, and the three subsequently more distal structures are fault-propagation folds. There are two fault-bend folds in the form of a duplex in the Northern Tashenkou region. One structure is visible at the surface and the other is in the subsurface evident by surface dip data and the divergence of the two structures to the east of the Piqiang fault. In the Medial Tashenkou region, there is a single fault-propagation fold with a trishear component. In the Southern Tashenkou region there is one main fault-propagation fold with a trishear component, and a burgeoning blind structure in the subsurface. This structure is beneath the Southern Tashenkou and has been modeled as a fault-propagation fold with a trishear component as well.

The overall shortening magnitude of the western Kepintage is 35.3 +/- 3.5 km, which provides a shortening rate of 1.8 +/-0.2 mm/yr. This rate is within range of previously determined shortening rates of 1.8 mm/yr (Allen et al, 1999) and 1-1.9 mm/yr (Yin et al., 1998). The Medial Tashenkou and Southern Tashenkou regions indicate shortening magnitudes of 12.9 +/- 1.3 mm/yr to 10.5 +/- 1.0 mm/yr, respectively. These magnitudes produce shortening rates of 3.2 +/- 0.3 mm/yr and 7.5 +/- 0.8 mm/yr, respectively. These rates are much faster than long-term rates in the western Kepintage belt, indicating an overall increase in shortening over the past several million years. The rate of shortening evident in the Southern Tashenkou region is similar to current geodetic data for the region; this suggests an increase in shortening rates just in the Quaternary.

Change in structural style form north to south is attributed to change in Neogene strata thickness, and possibly changes in shortening rates. The change in structural style along strike is attributed to a variation of thickness of post-Paleozoic strata. The strata thickness changes from 6-10 km thick in the Kashi Basin, to ~4 km within the western Kepintage, to 0-2 km in the eastern Kepintage, and back up to 7-8 km in the Aksu Re-entrant. The décollement horizon is different within the Kepintage fold and thrust belt. Décollement in the eastern and western Kepintage lies within an evaporite horizon within the Paleozoic strata (McKnight, 1994, Yin et al., 1998, Allen et al., 1999), yet it lies within an evaporite horizon above the Paleozoic strata in the Kashi basin (Scharer et al., 2004 and Heermance et al., 2008) and Aksu Re-entrant (Yin et al., 1998 and Hubert-Ferrari et al., 2005). The main difference (Figure 20) in the western Kepintage is the décollement horizon, thrust faulting breaks through Paleozoic strata in the western Kepintage, but not in the adjacent Kashi basin or Aksu Re-entrant. It appears that it is easier to propagate a fault through old, dense, hard rocks, producing fault-propagation folds. And it is easier to slide parallel to bedding when thrusting through young, soft rocks, producing fault-bend folds.

REFERENCES

Abdrakhmatov, K. Ye., Aldazhanov, B.H., Hagar, Hamburger, M. W., Herring, T.A., Kalabaev, K.B., Makarov, V.I., Molnar, P., Panasyuk, S.V., Prilepin, M.T., Reilinger, R.E., Sadybakasov, I.S., Souter, B.J., Trapeznikov, Yu. A., Tsurkov, V. Ye., Zubovich, A.V., 1996. Relatively recent construction of the Tien Shan inferred from GPSmeasurements of presen-day crustal deformation rates. Nature, 384

Allen, M.B., Windley B.F., Chi, Z., Zhong-Yan, Z., and Guang-Rei, W., 1991, Basin evolution within and adjacent to the Tien Shan Range, NW China. Journal of the Geological Society, London 148, 369-378.

Allen, M.B., Windley, B.F., and Chi, Z.,1993, Palaeozoic collisional tectonics and magmatism of the Chinese Tien Shan, central Asia. Tectonophysics, 220 89-115

Allen, M.B., and Vincent, S.J., 1999, Late Cenozoic tectonics of the Kepintage thrust zone: Interactions of the Tien Shan and Tarim Basin, northwest China. Tectonics, 18, 4, 639-654

Allmendinger, R.W., 2012, Fold Fault Forward, v. 6

Allmendinger, R.W., 1998, Inverse and forward numerical modeling of trishear fault-propagation folds. Tectonics, 17, 4, 640-656

Avouac, J.P., Tapponnier, P.,1993, Active thrusting and folding along the northern tien shan and late Cenozoic rotation of the Tarim relative to Dzungaria and Kazakhstan. Journal of Geophysical Research, 98, B4, 6755-6804

Bally A.W., Chou, I-Ming, Clayton, R., Eugster, H.P., Kidwell, S., Meckel, L.D., Ryder, R.T., Watts, A.B., Wilson, A.A., 1986, Notes of Sedimentary Basins in China – Report of the American Sedimentary Basin Delegation to the People's Republic of China, Dept of the Interior, USGS, 86-327

Butler, R.W.H., Tavarnelli, E., and Grasso, M., 2006, Structural inheritance in mountain belts: An Alpine-Apennine perspective. Journal of Structural Geology, 28, 1893-1908

Carroll, A.R., Graham, S.A., Hendrix, M.S., Ying, D., and Zhou, D., 1995, Late Paleozoic tectonic amalgamation of northwestern China: Sedimentary record of the northern Tarim, northwestern Turpan, and southern Junggar Basins. GSA Bulletin, 107, 5, 571-594

Cristallini, E.O., Allmendinger, R.W., 2002, Backlimb trishear: a kinematic model for curved folds developed over angular fault-bends. Journal of Stuctural Geology, 24, 2, 289-295

Dahlen, F.A., 1990, Critical Taper Model of Fold-and-Thrust Belts and Accretionary Wedges. Annual Review of Planetary Sciences, 18, 55

Davis, D., Suppe, J., and Dahlen, F.A., 1983, Mechanics of Fold-and-Thrust Belts and Accretionary Wedges. Jurnal of Geophysical Research, 88, B2, 1153-1172

Dumitru, T.A., Zhou, D., Chang, E.Z., Graham, S.A., Hendrix, M.S., Sobel, E.R., and Carroll, A.R., 2001, Uplift, exhumation, and deformation in the Chinese Tian Shan. GSA Memoir 194, 71-99

Dupont-Nivet, G. and Krijgsman, W., 2012, Magnetostratigraphic methods and applications. Tectonics of Sedimentary Basins – Recent Advances (textbook). 4, 80

Erslev, E., 1991, Trishear fault-propagation folding. Geology, 19, 617-620

Epard, J.L., Groshong Jr., R.H., 1995, Kinematic model of detachment folding including limb rotation, fixed hinges and layer-parallel strain. Tectonophysics, 247, 85-103

GeoMapApp: http://www.geomapapp.org

Ghose, S., Mellors, R.J., Korjenkov, A.M., Hamburger, M.W., Pavlis, T.L., Pavlis, G.L., Omuraliev, M., Mamyrov, E., and Muraliev, A.R., 1997, The Ms = 7.3 1992 Suusamyr, Kyrgyzstan, earthquake in the Tien Shan: 2. Aftershock focal mechanisms and surface deformation. Seismological Society of America

Hardy, S. and Ford, M., 1997, Numerical modeling of trishear propagation folding. Tectonics, 16, 5, 841-854

Heermance, R.V., Chen, J., Burbank, D.W., and Wang, C., 2007, Chronology and tectonic controls of Late Tertiary deposition in the southwestern Tian Shan foreland, NW China. Basin Research, 19, 599-632

Heermance, R.V., Chen, J., Burbank, D.W., and Miao, J., 2008, Temporal constraints and pulsed Late Cenozoic deformation during the structural disruption of the active Kashi foreland, northwest China. Tectonics, 27

Hendrix, M.S., Dumitru, T.A., Graham, S.A., 1994, Late Oligocene-early Miocene unroofing in the Chinese Tian Shan: An early effect of the India-Asia collision. Geology, 22, 487-490

Hubert-Ferrari, A., Suppe, J., Van Der Woerd, J., and Wang, X., 2005, Irrehular earthquake cycle along the southern Tianshan front, Aksu area, China. Journal of Geophysical Research., 110

Hubert-Ferrari, A., Suppe, J., Gonzalez-Mieres, R., and Wang, X., 2006, Mechanisms of active folding of the landscape (southern Tian Shan, China). Journal of Geophysical Research, 12

Iaffa, D. N., Sàbat, F., Muñoz, J.A., Mon, R., Gutierrez, A.A., 2011, The role of inherited structures in a foreland basin evolution. The Metán Basin in NW Argentina. Journal of Structural Geology, doi:10.1016/j.jsg.2011.09.005

Lujan, M., Storti, F., Bananya, J., Crespo-Blanc, A., Rossetti, F., 2003, Role of decollement material with different rheological properties in the structure of the Aljibe thrust imbricate (Flysch Trough, Gibraltar Arc): an analogue modeling approach. Journal of Structural Geology, 25, p. 867-881

McKnight, C.L., 1993, Structural styles and tectonic significance of the Tian Shan foothill fold and thrust belts, northwest China. Ph.D Thsis, 207 pp,. Stanford University, Stanford, California

Molnar, P., and Tapponnier, P., 1975, Conozoic Tectonics of Asia: Effects of a Continental Collision. Science, 189, 4201

Nishidai, T. and Berry, J.L., 1990, Structure and hydrocarbon potential of the Tarim Basin (NW China) from satellite imagery. Journal of Petroleum Geology, 13, 35-58

Regalla, C., Fisher, D., Kirby, E., 2010, Timing and magnitude of shortening within the inner fore arc of the Japan Trench. Journal of Geophysical Research, 115

Reigber, Ch., Michel, G. W. et al., 2001, New space geodetic constraints on the distribution of deformation in Central Asia. Earth and Planetary Science Letters, 191, 157–165.

Riba, O., 1976, Syntectonic unconformities of the Alto Cardener, Spanish Pyrenees: A genetic interpretation. Sedimentary Geology, 15, 213-233

Ryan, W.B.F., Carbotte, S.M., Coplan, J.O., O'Hara, S., Melkonian, A., Arko, R., Weissel, R.A., Ferrini, V., Goodwillie, A., Nitsche, F., Bonczkowski, J., and Zemsky, R., 2009, Global Multi-Resolution Topography synthesis, Geochem. Geophys. Geosyst., 10, Q03014, doi:10.1029/2008GC002332

Scharer, K.M., Burbank, D.W., Chen, J., Weldon, R.J., Rubin, C., Zhao, R., Shen, J., 2004, Detachment folding in the Southwestern Tian Shan – Tarim foreland, China: shortening estimates and rates. Journal of Structural Geology, 26, 2119-2137

Sepehr, M. and Cosgrove, J.W., 2004, Structural framework of the Zagros Fold-Thrust Belt, Iran. Marine and Petroleum Geology 21, 829-843

Sobel, E.R., Dumitru, T.A., 1997, Thrusting and exhumation around the margins of the

western Tarim basin during the India-Asia collision, Journal of Goephysical Research, 102, B3, 5043

Sobel, E.R., Chen, J., Heermance, R.V., 2006, Late Oligocene-Early Miocene initiation of shortening in the Southwestern Chinese Tian Shan: Implications for Neogene shortening rate variations. Earth and Planetary Science Letters, 247, 70-81

Sun, J., R. X. Zhu, and Bowler, J.,2004, Timing of the Tianshan Mountains uplift constrained by magne- tostratigraphic analysis of molasse deposits, Earth Planet. Sci. Lett., 219, 239–253

Suppe, J., Chou, G.T., Hook, S.C.,1992, Rates of folding and faulting determined from growth strata. In: McClay, K.R. (Ed.), Thrust Tectonics. Chapman & Hall, Suffolk, 105 – 121.

Suppe, J., Sabat, F., Muñoz, J.A., Poblet, J., Roca, E., Verges, J., 1997, Bed-by-bed growth by kink-band migration: Sant Llorenç de Morunys, eastern Pyrenees. Journal of Structural Geology, 19, 3-4, 443-461ç

Suppe, J., Connors, C.D., Zhang, Y., 2004, Shear Fault-bend Folding, in K.R. McClay, ed., Thrust tectonics and hydrocarbon systems: AAPG Memoir 82, 303-323

Turner, S.A., Cosgrove, J.W., and Liu, J.G., 2010, Controls on lateral structural variability along the Keping Shan Thrust Belt, SW Tien Shan Foreland, China. Geologic Society, London, Special Publications, 348, 71-85

Vandenberghe, J., Zhisheng, A., Nugteren, G., Huayu, L., and Huissteden, K. Van,1997, New absolute time scale for the Quaternary climate in the Chinese loess egion by grain-size analysis. Geology, 25, 1, 35-38

Verges, J., Marzo, M., Munoz, J.A., 2002, Growth strata in foreland settings. Sedimentary Geology 146 1-9

Yang, S., Jie, L., Wang, Q., 2008, The deformation pattern and fault rate in the Tianshan Mountains inferred from GPS observations, Science in China Series D: Earth Sciences, 51, 8, 1064-1080

Yin, A., Nie, S., Craig, P., and Harrison, T.M.,1998, Late Cenozoic tectonic evolution of the southern Chinese Tian Shan. Tectonics,17, 1, 1-27

Yin, A., Rumelhart, P.E., Butler, R., Cowgill, E., Harrison, T.M, Foster, D.A., Ingersoll, R.V., Qing, Z., Xian-Qiang, Z., Xiao-Feng, W., Hanson, A., Raza, A, 2002, Tectonic history of the Altyn Tagh fault system in northern Tibet inferred from Cenozoic sedimentation, GSA Bulletin, 114, 10, 1257-1295

Zubovich, A.V., Wang, X., Scherba, Y.G., Scholochkov, G.G., Reilinger, R., Reigner, C., Mosienko, O.I., Molnar, P., Michajljow, W., Makarov, V.I., Li, J., Kuzikov, S.I., Herring, T.A., Hamburger, M.W., Hager, B.H., Dang, Y., Bragin, V.D., Beisenbaev, R.T., 2010, GPS velocity field for the Tien Shan and surrounding regions. Tectonics, 29, TC6014

APPENDIX A: FIGURES

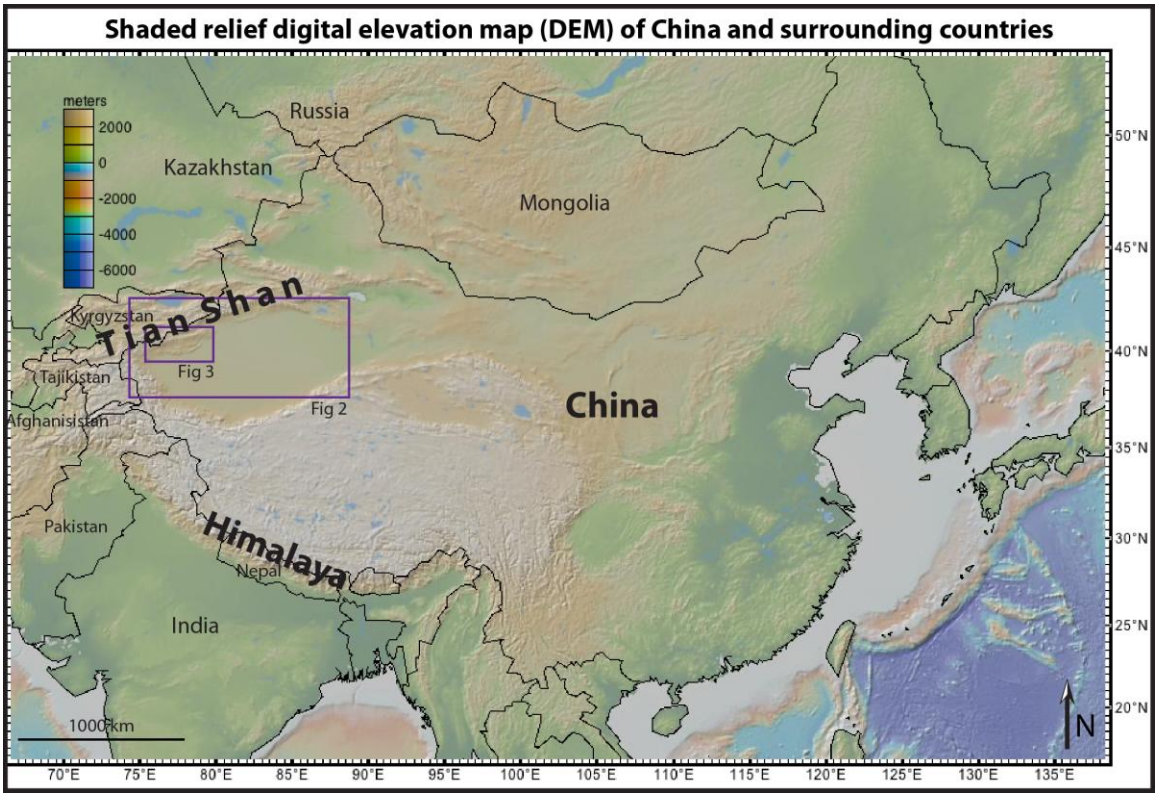

Figure 1 - Shaded relief digital elevation map indicating the area of interest, the Kashi-Aksu thrust system of the Tian Shan foreland in northwestern China. The Tian Shan and Himalaya Ranges are shown. Black lines represent country borders. Purple boxes indicate Figure 2 and Figure 3. (DEM courtesy of geomapapp.org)

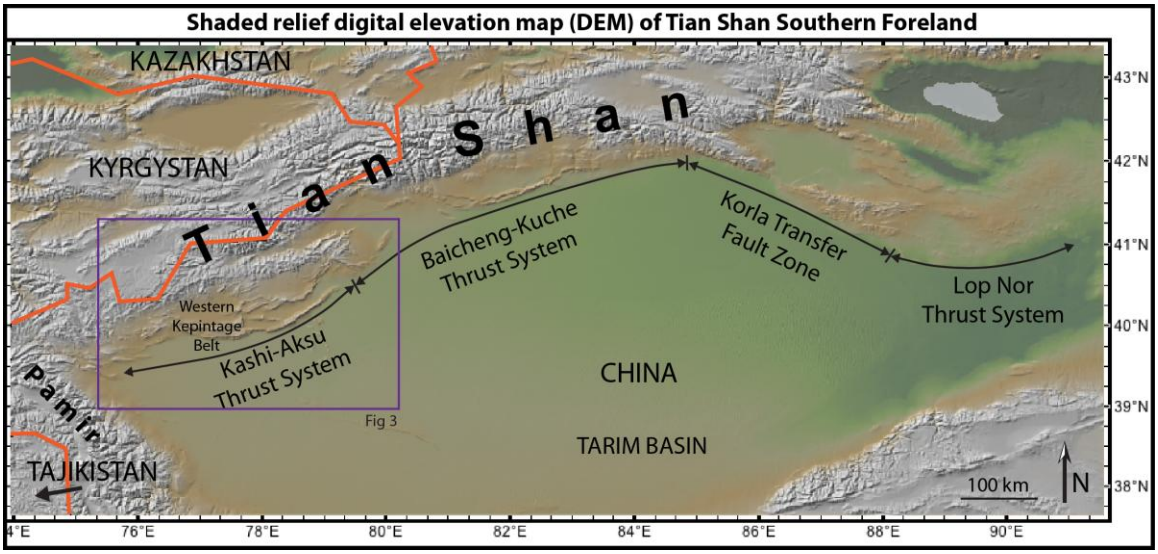

Figure 2 - Shaded relief digital elevation map showing the extent of the Tian Shan foreland. Orange lines represent country borders. Purple box indicates Figure 3. (DEM courtesy of geomapapp.org)

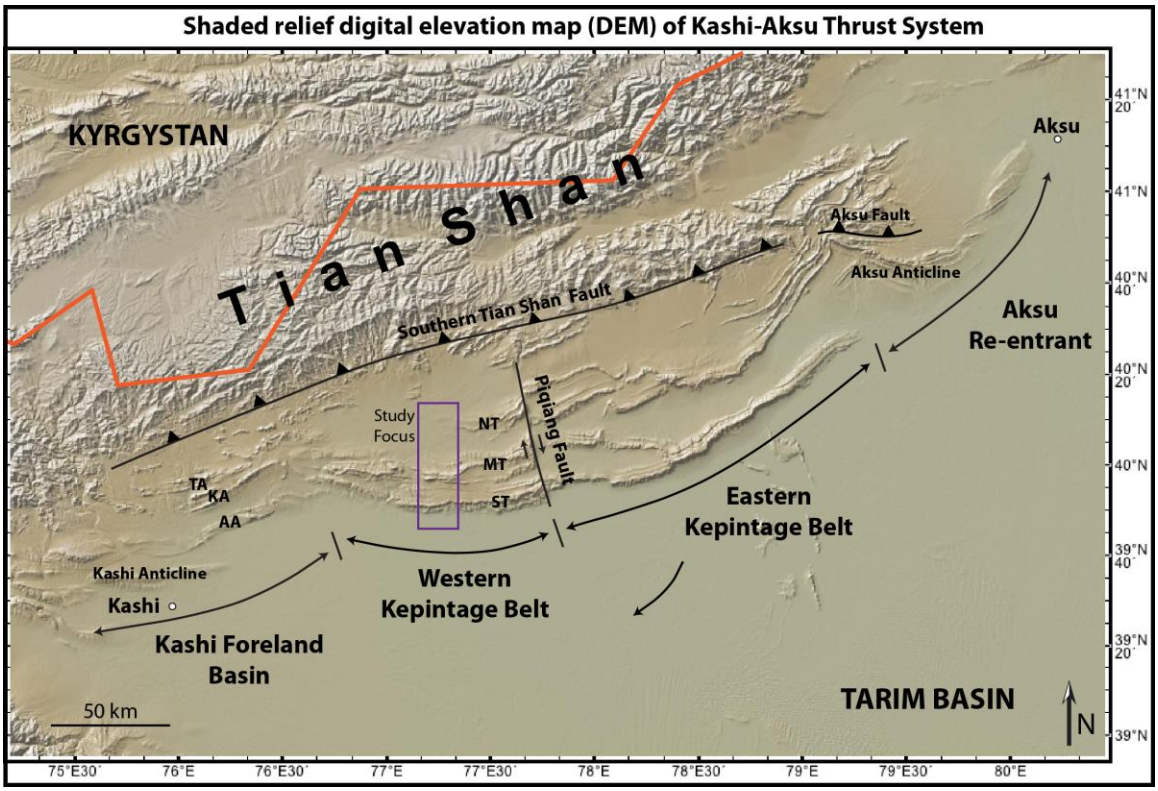

Figure 3 - Shaded relief digital elevation map of the Kashi-Aksu Thrust System. Orange line represents country borders. Main cities (Kashi and Aksu) of the Kashi-Aksu Thrust System are shown. Piqaing Fault divides the western and eastern segments of the Kepintage belt. TA – Tashipishake Anticline, KA – Keketamu Anticline, AA – Atushi Anticline, NT – Northern Tashenkou region, MT – Medial Tashenkou region, ST – Southern Tashenkou region. (DEM courtesy of geomapapp.org)

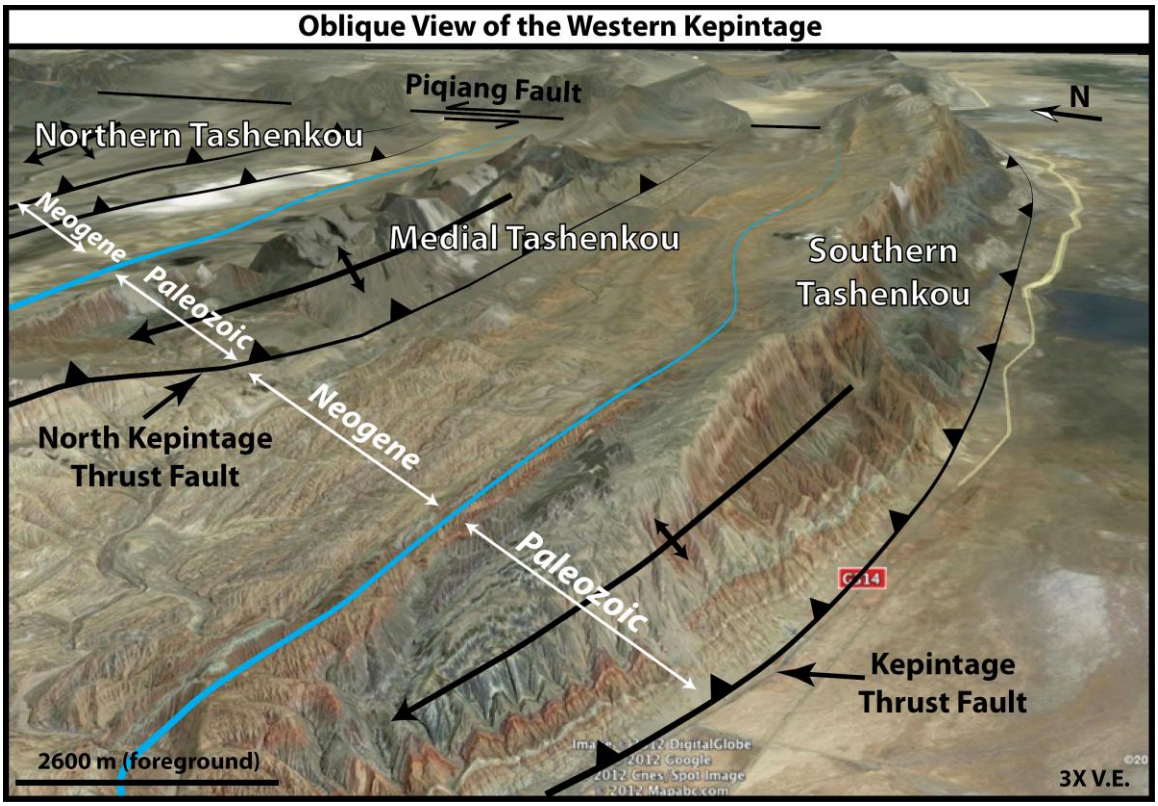

Figure 4 - Oblique view of the western Kepintage. Three main structures identified, and extent of Paleozoic and Neogene strata shown. Blue lines indicate boundary between each region. (map courtesy of Google Earth)

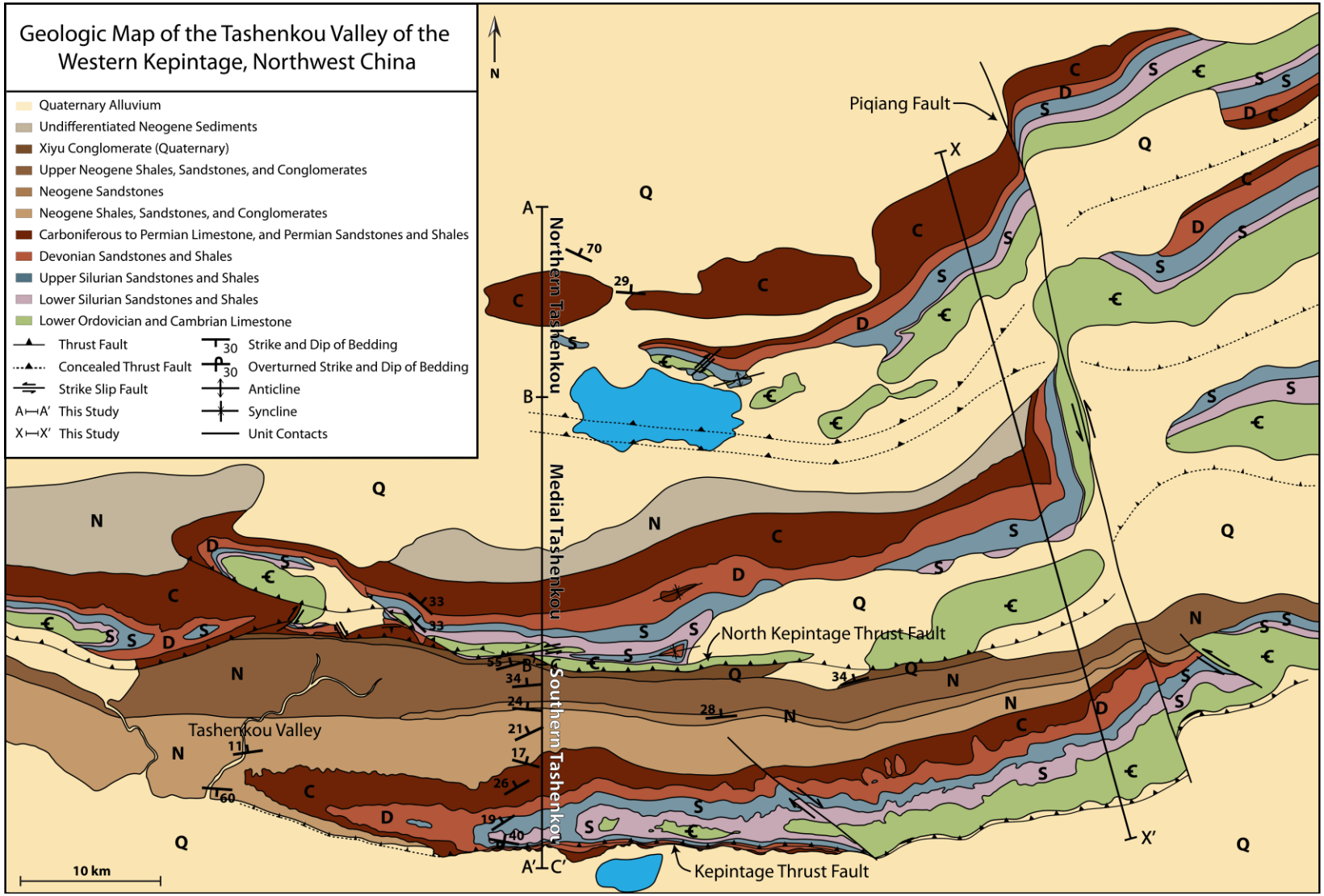

Figure 5 - Geologic map of the western Kepintage. Structures named for the Tashenkou river drainage.

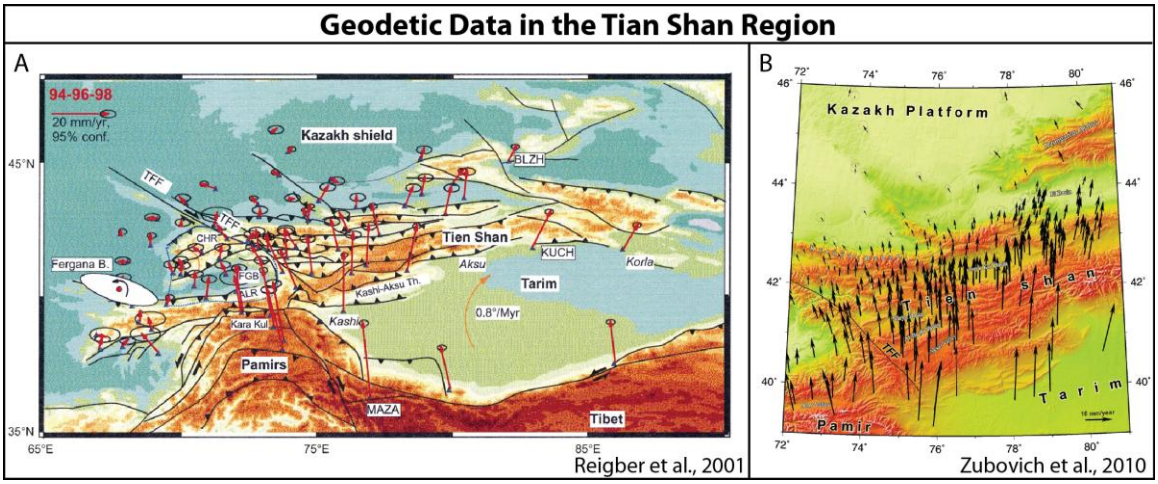

Figure 6 – Geodetic data in the Tian Shan region. A) Geodetic data from Reigber et al., 2001. Geodetic data suggests a shorting rate of 8 +/-3 mm/yr. B) Geodetic data from Zubovich et al., 2010. Geodetic data suggests a shorting rate of 4-7 mm/yr.

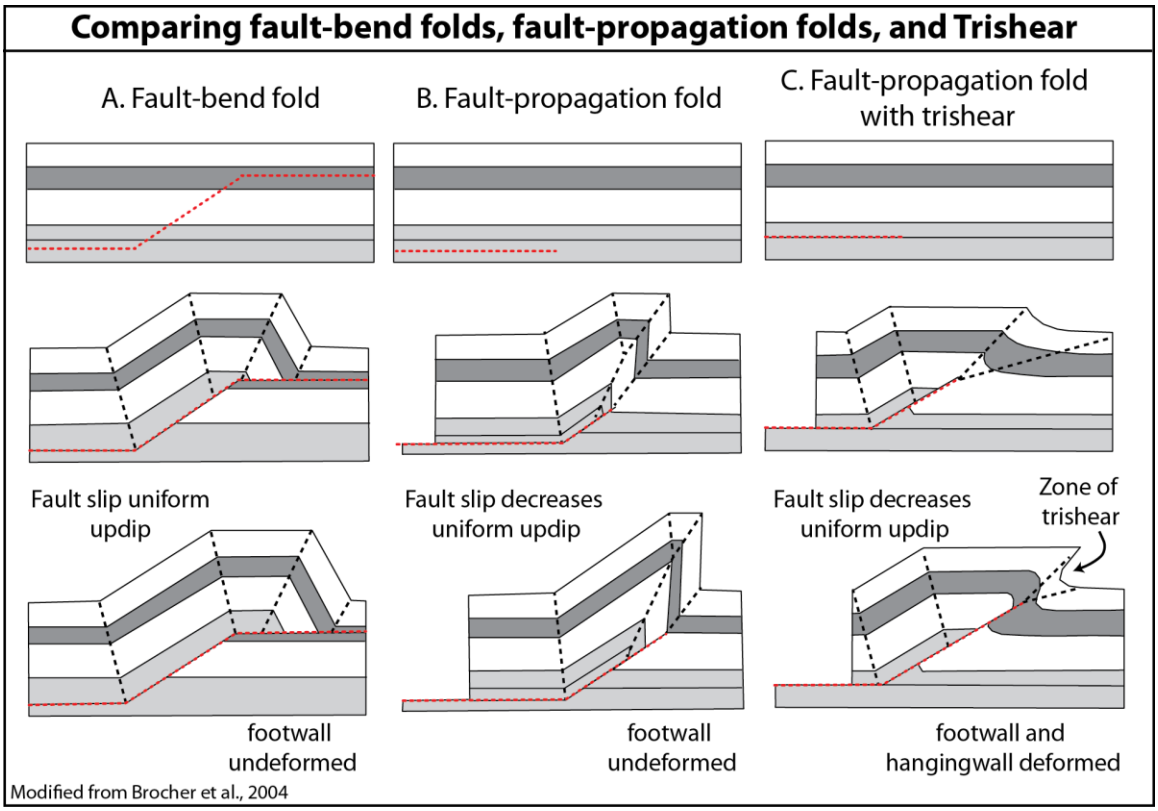

Figure 7 – Comparing structural styles. A) Fault-bend fold, uniform slip updip, no overturned strata. B) Fault-propagation fold, slip decreases updip, can have overturned strata in forelimb. C) Fault-propagation fold with trishear component, slip decreases updip, can have overturned strata in forelimb, triangle zone (trishear) of shear deformation at the fault tip

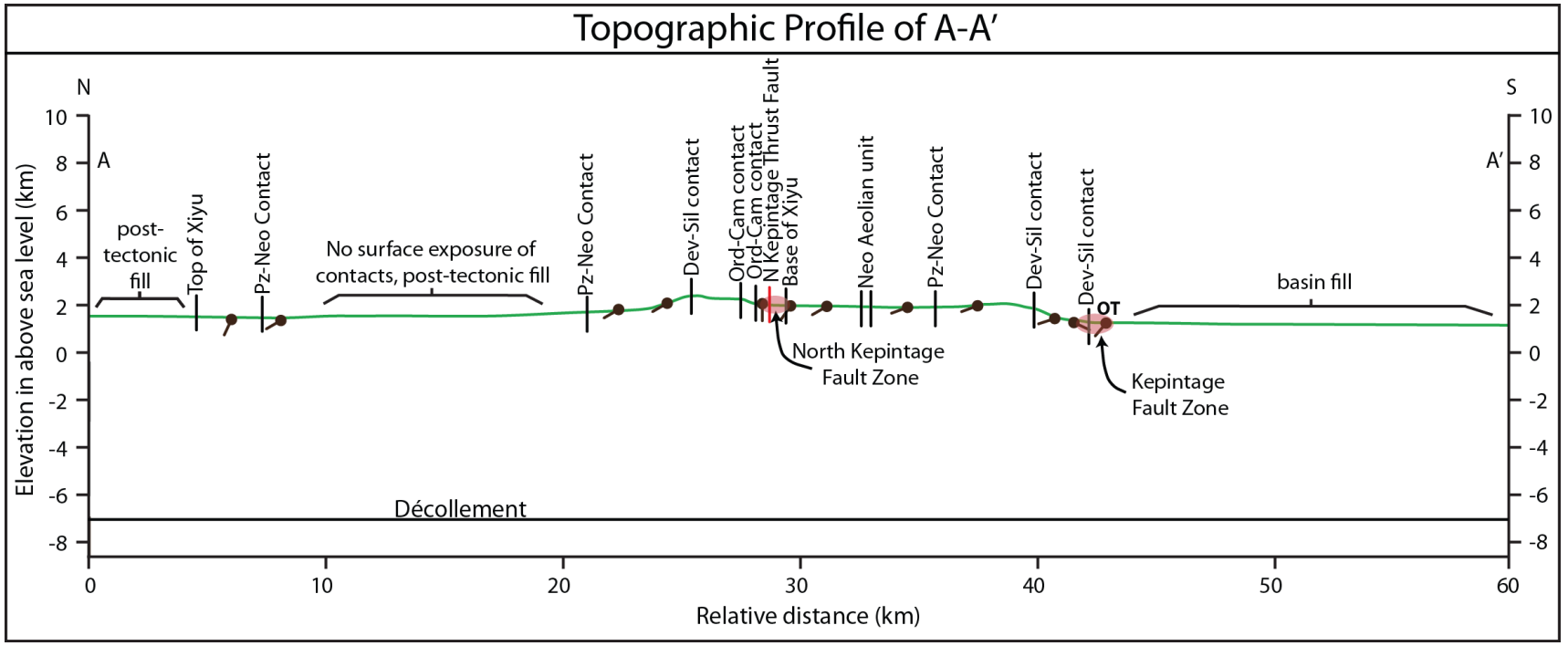

Figure 8 – Topographic profile of A-A' illustrating dip data, fault locations, stratigraphic contacts, and depth to décollement. Green line is the topographic profile from A to A', black tick marks are stratigraphic contacts, red tick is discrete fault, red ovals are fault zones.

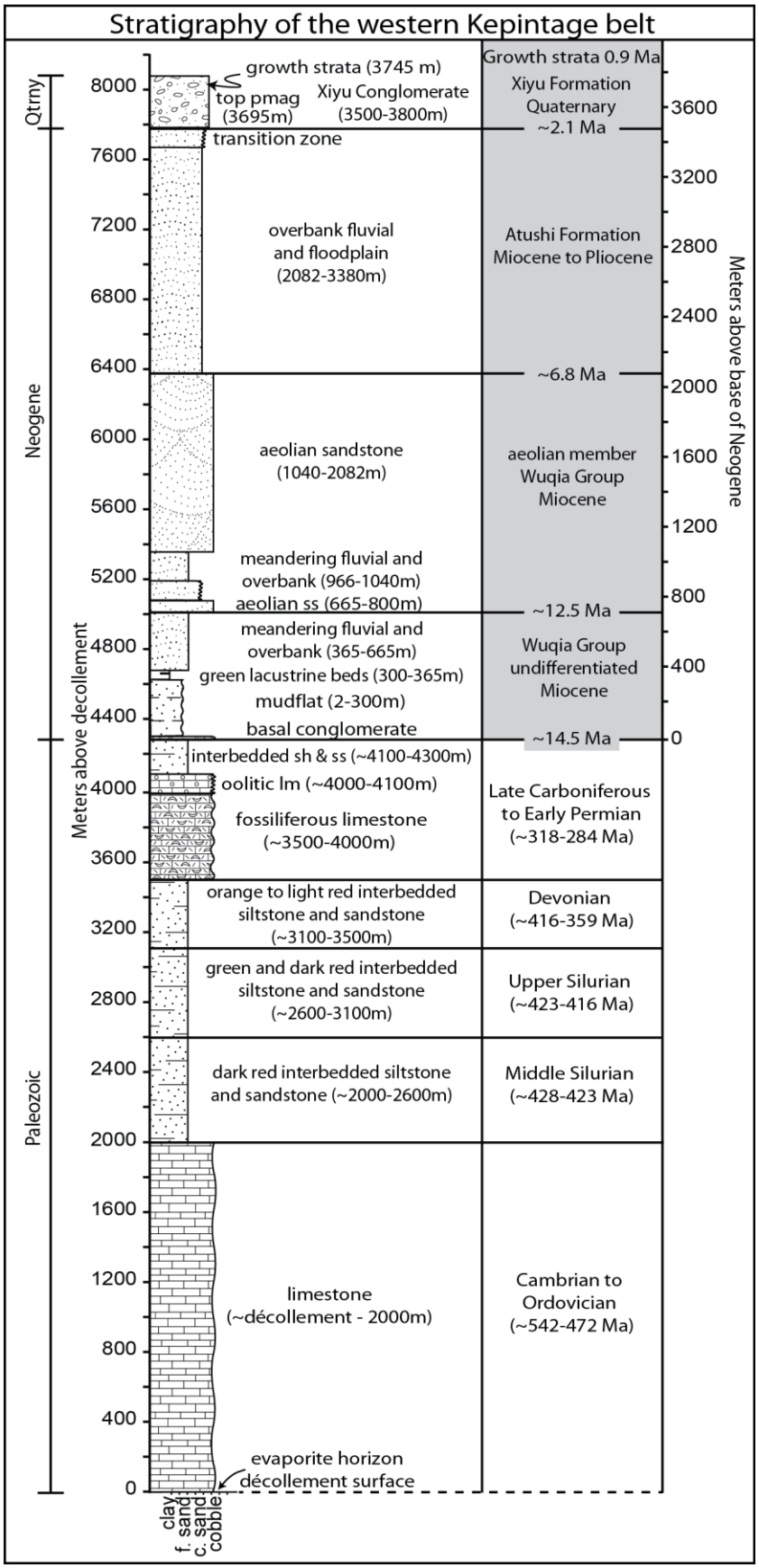

Figure 9 - Composite stratigraphic column of the western Kepintage fold and thrust belt. Depths, thickness, and description of Paleozoic stratigraphy are based on field strike and dip measurements, calculated thicknesses, and previously published literature. Neogene stratigraphy was measured in the field with a Jacob Staff and Abney Level. Neogene ages are from correlation of stratigraphy in the western Kepintage to the Kashi Basin. Scale on the left is the approximate measured stratigraphic height above décollement. Scale to the right is measured height above Neogene-Paleozoic contact.

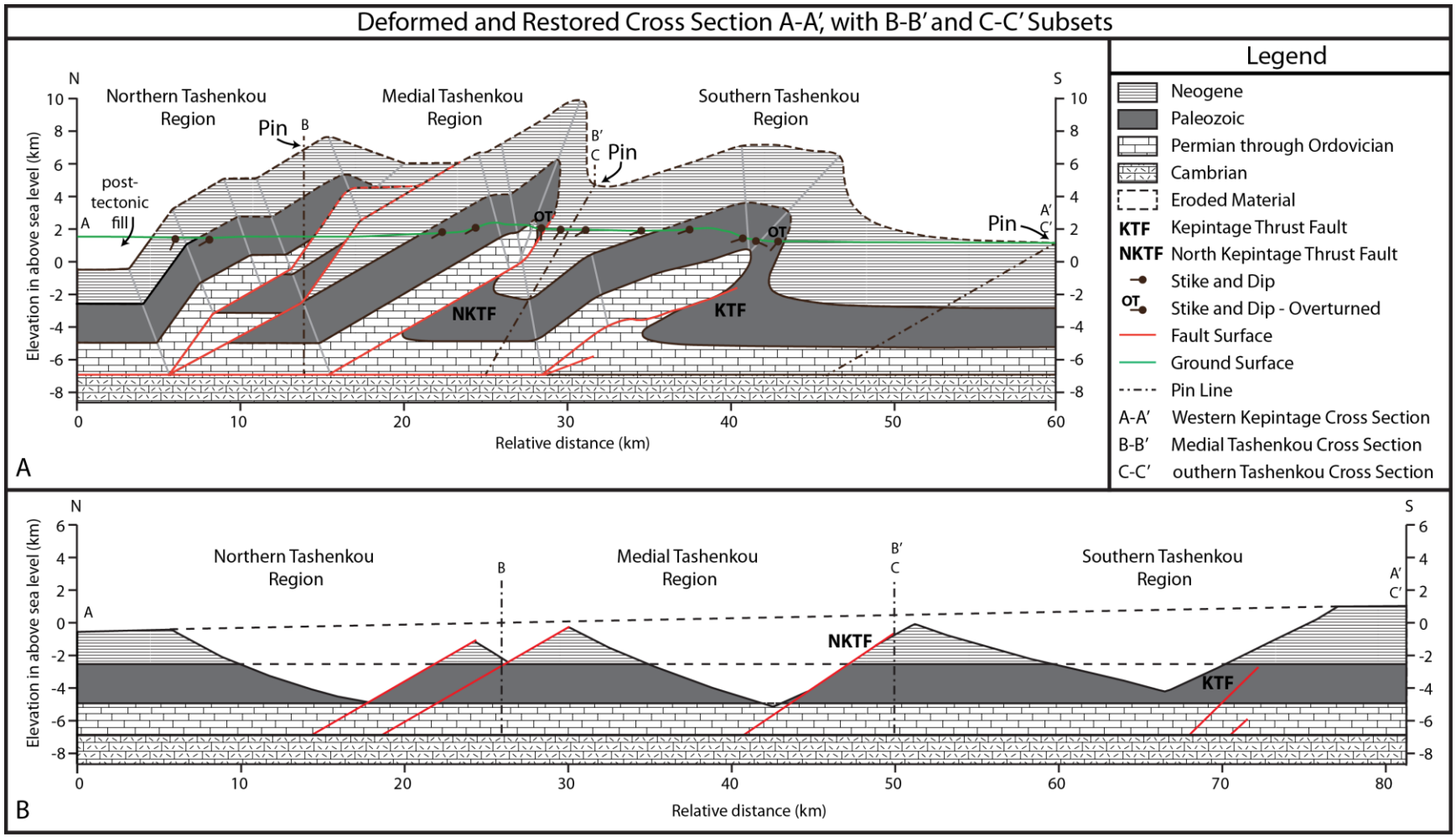

Figure 10 caption of following page.

Figure 10 - Cross section through the western Kepintage. A) A-A' is through all structures. B-B' is through the Medial Tashenkou region. C-C' is through the Southern Tashenkou region. Pin lines are tilted at 30° and 60° to compensate for trishear in the Medial Tashenkou and Southern Tashenkou regions, respectively. B) Area restored cross section. Neogene strata thin to the north. The Medial Tashenkou and Southern Tashenkou regions both have a trishear angle of 60°, this must be accounted for when restoring the cross section. The shear component is evenly distributed in the hanging wall and the footwall in order to maintain conservation of mass (Erslev, 1991). It is necessary to tilt the trailing pin line to account for the shear component. Since shear is evenly distributed to the hanging wall and footwall, tilting the pin-line after the first trishear structure, in the Medial Tashenkou region, by 30° (or half the trishear angle) will correct for the shear in this structure. Then tilting the pin-line after the structure in the Southern Tashenkou region by 60° (half of the trishear angle in the Southern Tashenkou region plus half of the shear in the Medial Tashenkou region), will correct for shear in this structure. Instead of the pin-line being straight and perpendicular in the deformed cross section, it is tilted in the restored cross section and straight and perpendicular in the deformed section.

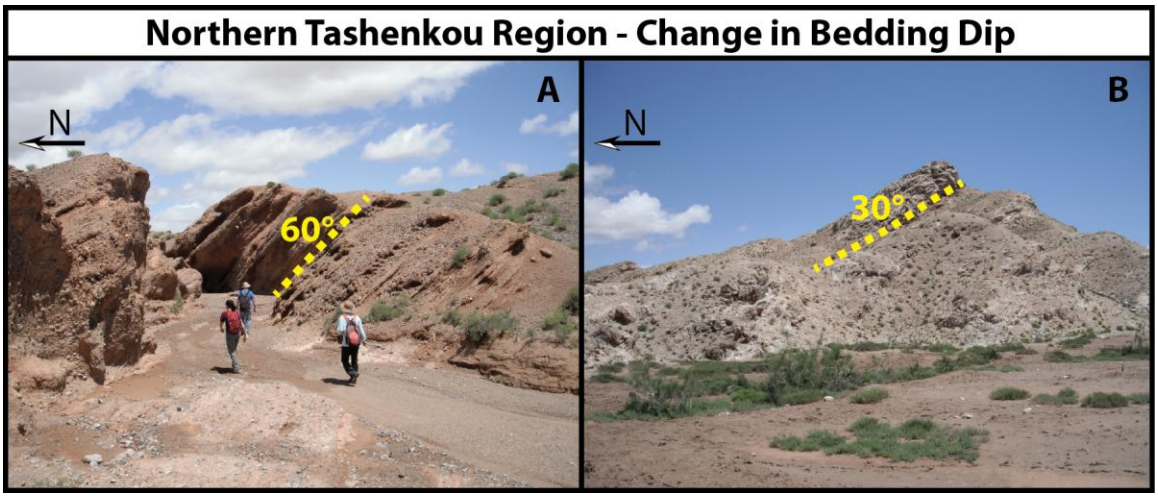

Figure 11 – Northern Tashenkou Region. A) Bedding is dipping approximately 60°-70° to the north. B) Bedding is dipping approximately 30° to the north. Location A is approximately 1 km north of location B.

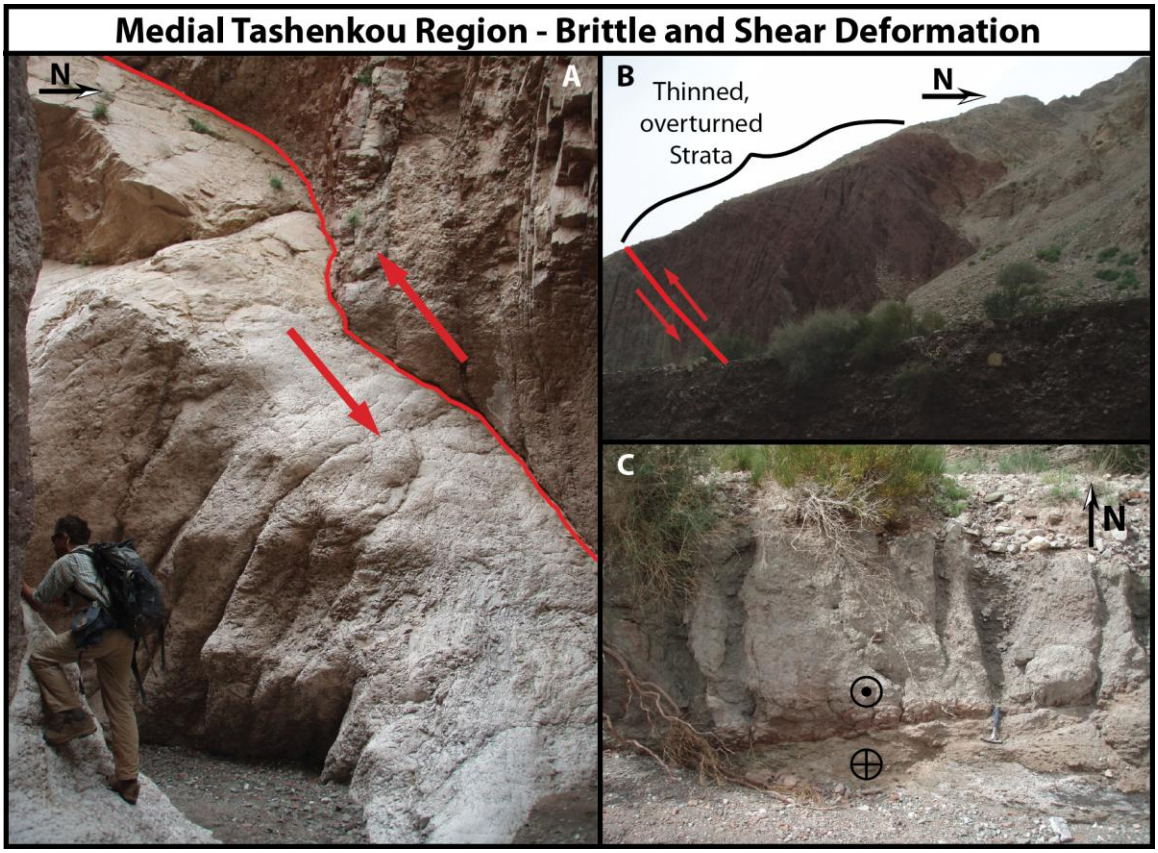

Figure 12 – Medial Tashenkou region. A) Discrete faulting in Paleozoic Limestone. B) Structurally thinned and overturned Silurian strata. C) Fault gouge. Paleozoic strata thrust over Quaternary strata. Location A and C are approximately 100 meters apart, location B is in between A and C.

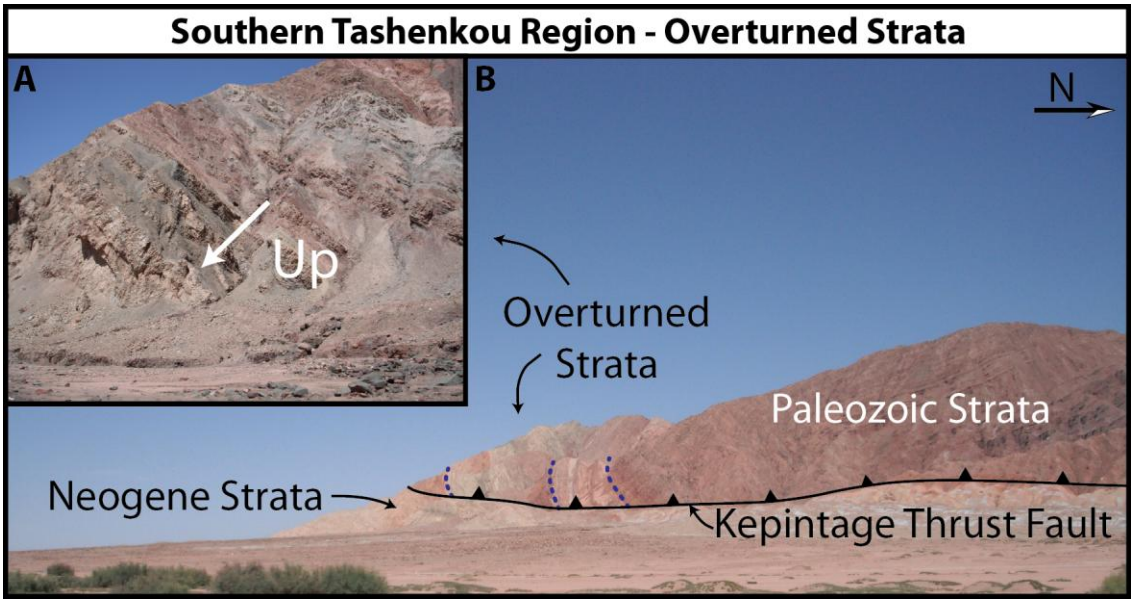

Figure 13 – Southern Tashenkou region. A) Overturned strata near the Kepintage Thrust Fault. B) Paleozoic strata thrust over Neogene strata; overturned strata delineated with blue dashed lines.

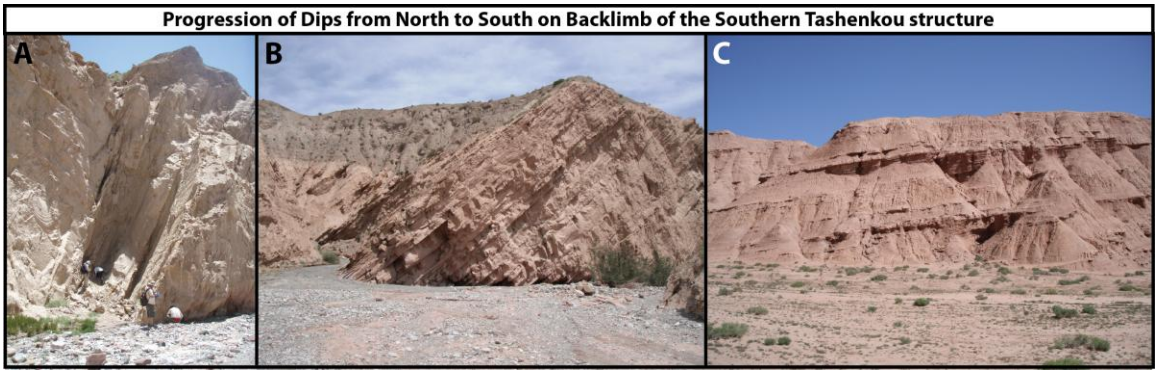

Figure 14 – Southern Tashenkou region progression of dips of Neogene strata between the North Kepintage Thrust Fault and the crest of the Southern Tashenkou structure. A) strata are dipping approximately 65° degrees to the north, B) strata are dipping approximately 40° degrees to the north, C) strata are dipping approximately 10° to the north.

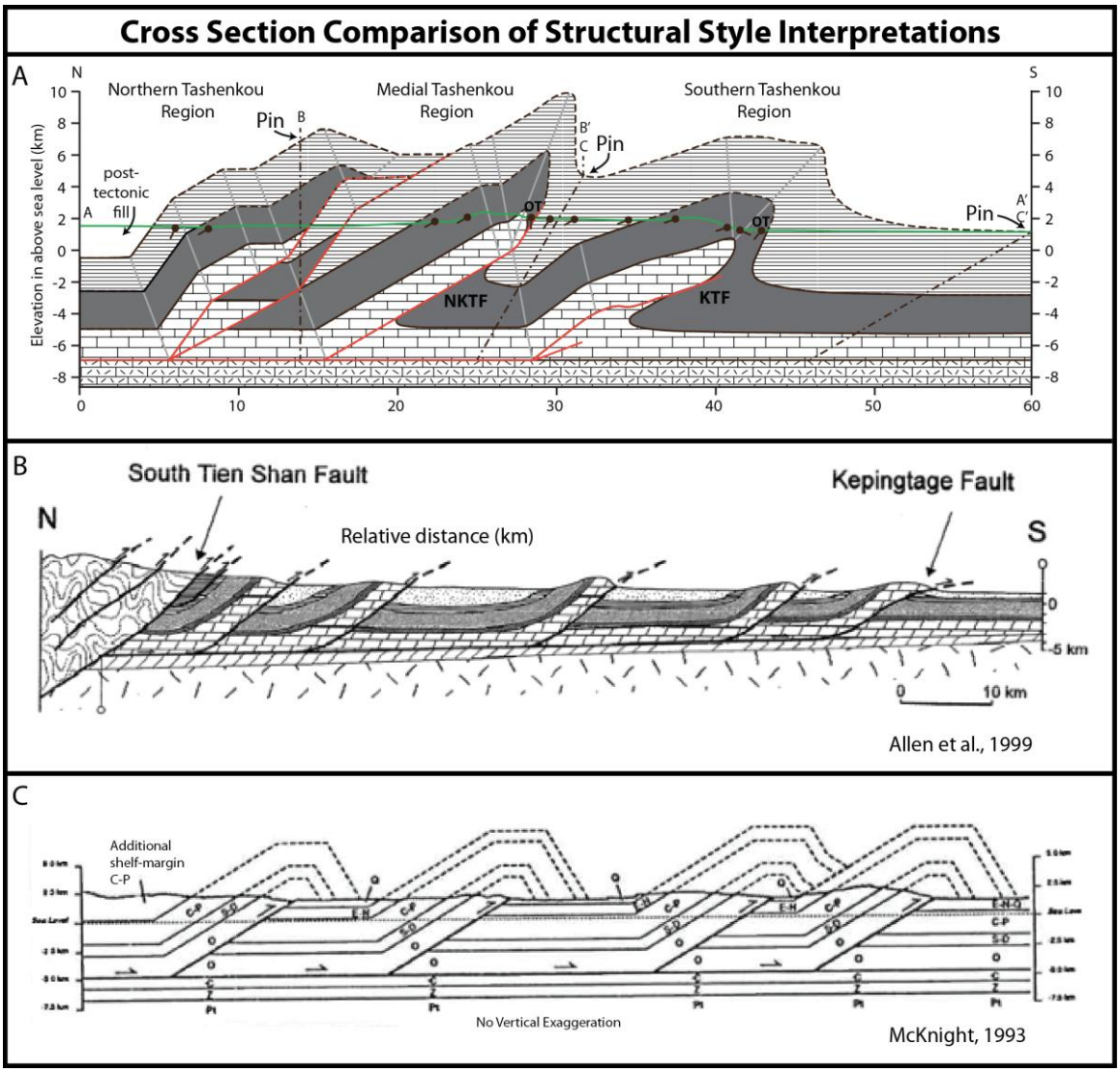

Figure 15 – Cross section comparison of structural style interpretations. A) Cross section from this study indicating fault-bend folds, and fault-propagation folds with a trishear component. B) Cross section from Allen et al., 1999 indicating all fault-propagation folds. C) Cross section from McKnight, 1993 indicating all fault-bend folds. Neither cross sections B or C recognize a buried structure or a change in structural style normal to strike.

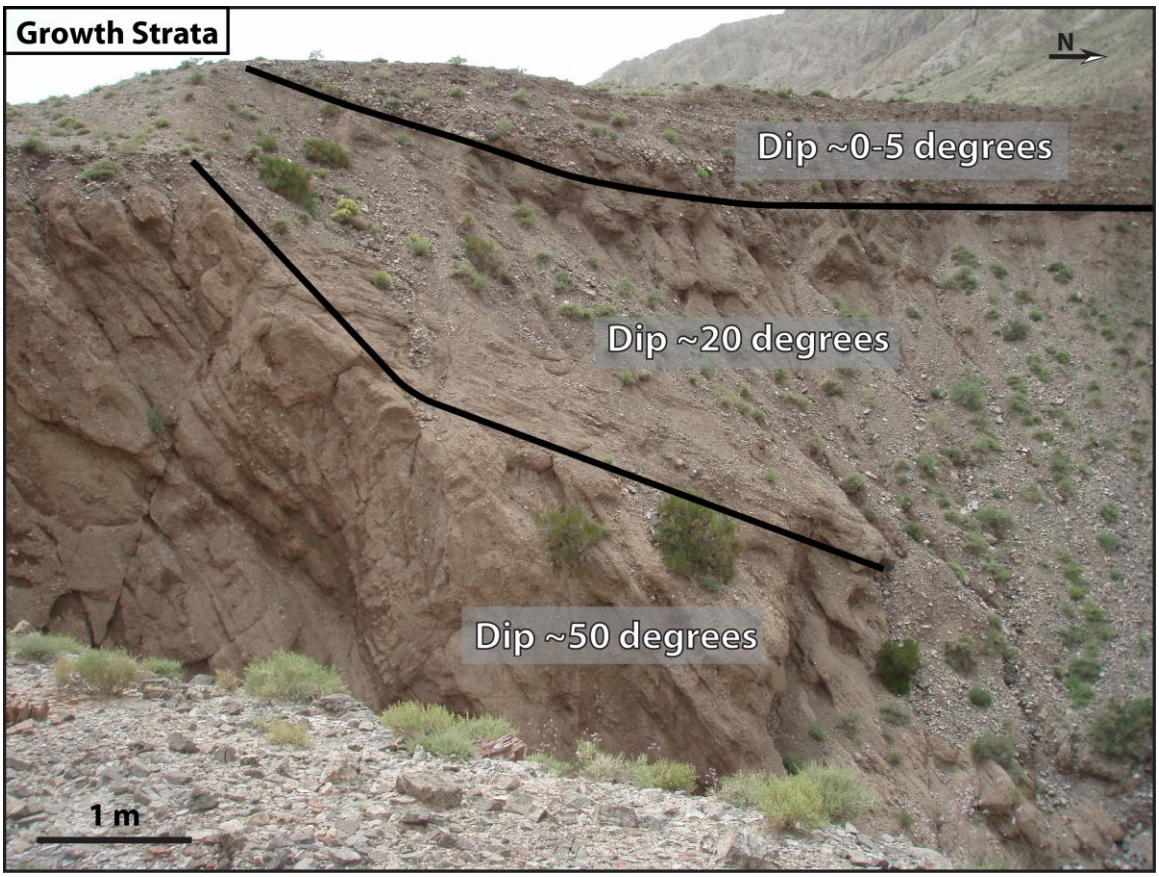

Figure 16 - Growth strata observed on the backlimb of the Southern Tashenkou fault-propagation fold near the North Kepintage Thrust Fault. Strata exhibit the characteristic fanning associated with growth strata. Growth strata is at the top of the Xiyu Conglomerate.

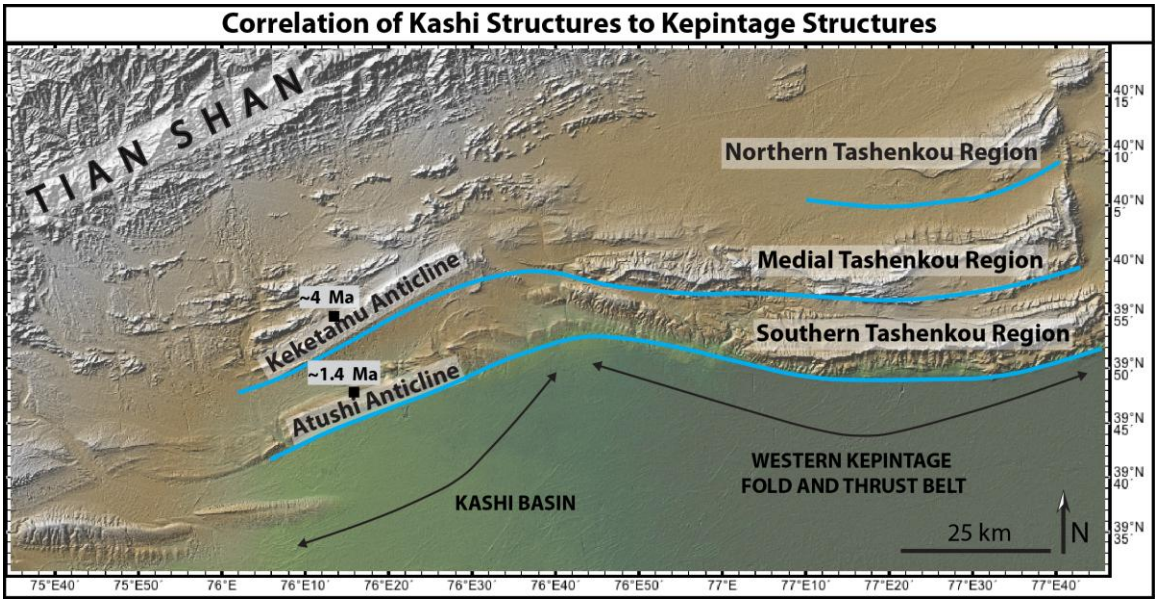

Figure 17 - Shaded relief digital elevation map of the western Kepintage and Kashi basin. Medial Tashenkou and Southern Tashenkou regions are correlative to the Keketamu and Atushi Anticlines, respectively. Ages in Kashi Basin from growth strata and magnetostratigraphy (Heermance et al., 2007).

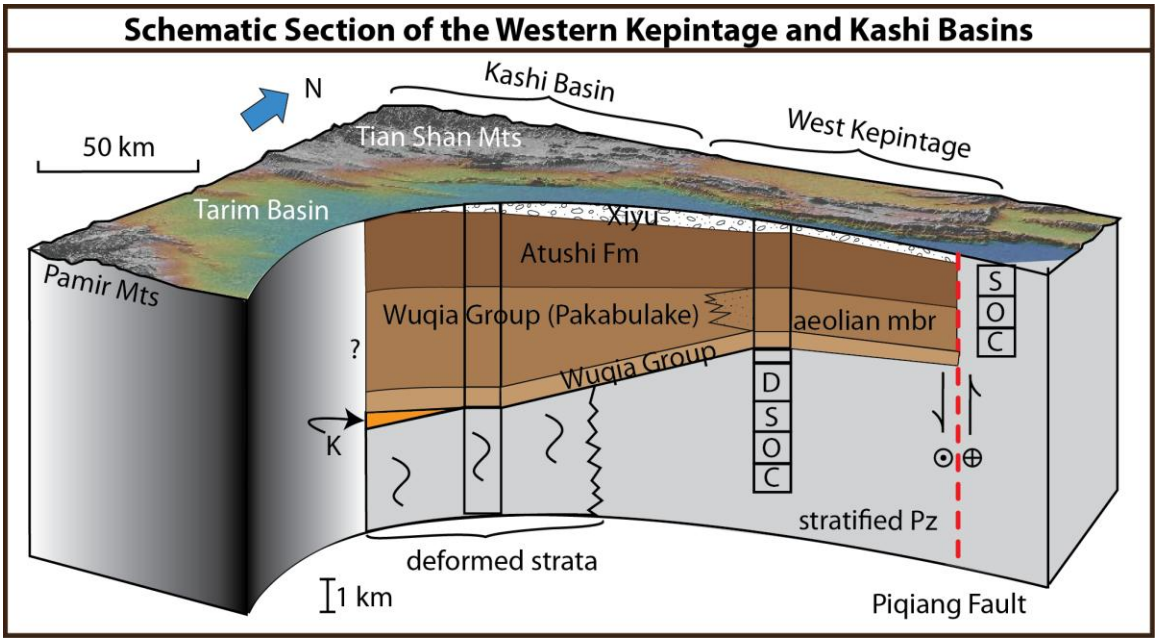

Figure 18 - Schematic section of the western Kepintage and Kashi Basins. This figure illustrates the correlation of strata across the segments, as well as the change in stratigraphic thickness across the segments and the Piqiang Fault.

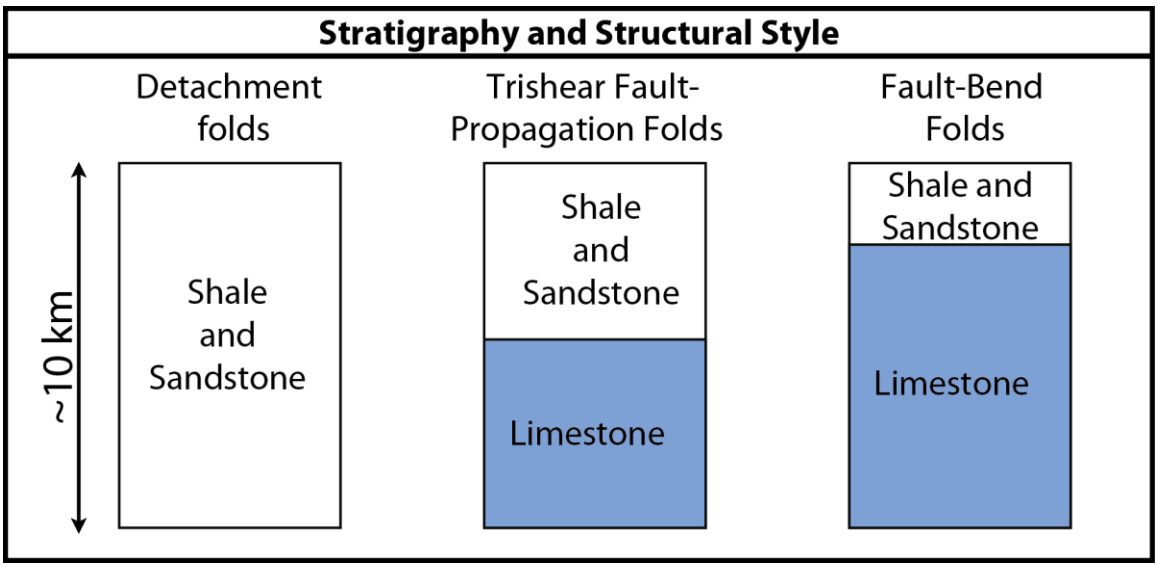

Figure 19 – Schematic of the relationship between stratigraphy and structural style. Where the strata above the décollement are dominated by relatively young (Neogene) sandstones and shales, detachment folds dominate as in the Kashi Basin (Heermance et al., 2008) and Aksu Re-entrant (Hubert-Ferrari et al., 2005). Where the strata above the décollement are approximately half relatively young (Neogene) sandstones and shales and half old (Paleozoic) limestone and other shallow marine sediments, fault-propagation folds with a trishear component dominate as in Medial Tashenkou and Southern Tashenkou regions (this study). Where the strata above the décollement are approximately a quarter relatively young (Neogene) sandstones and shales and three quarters old (Paleozoic) limestone and other shallow marine sediments, fault-bend folds dominate as in Northern Tashenkou region (this study).

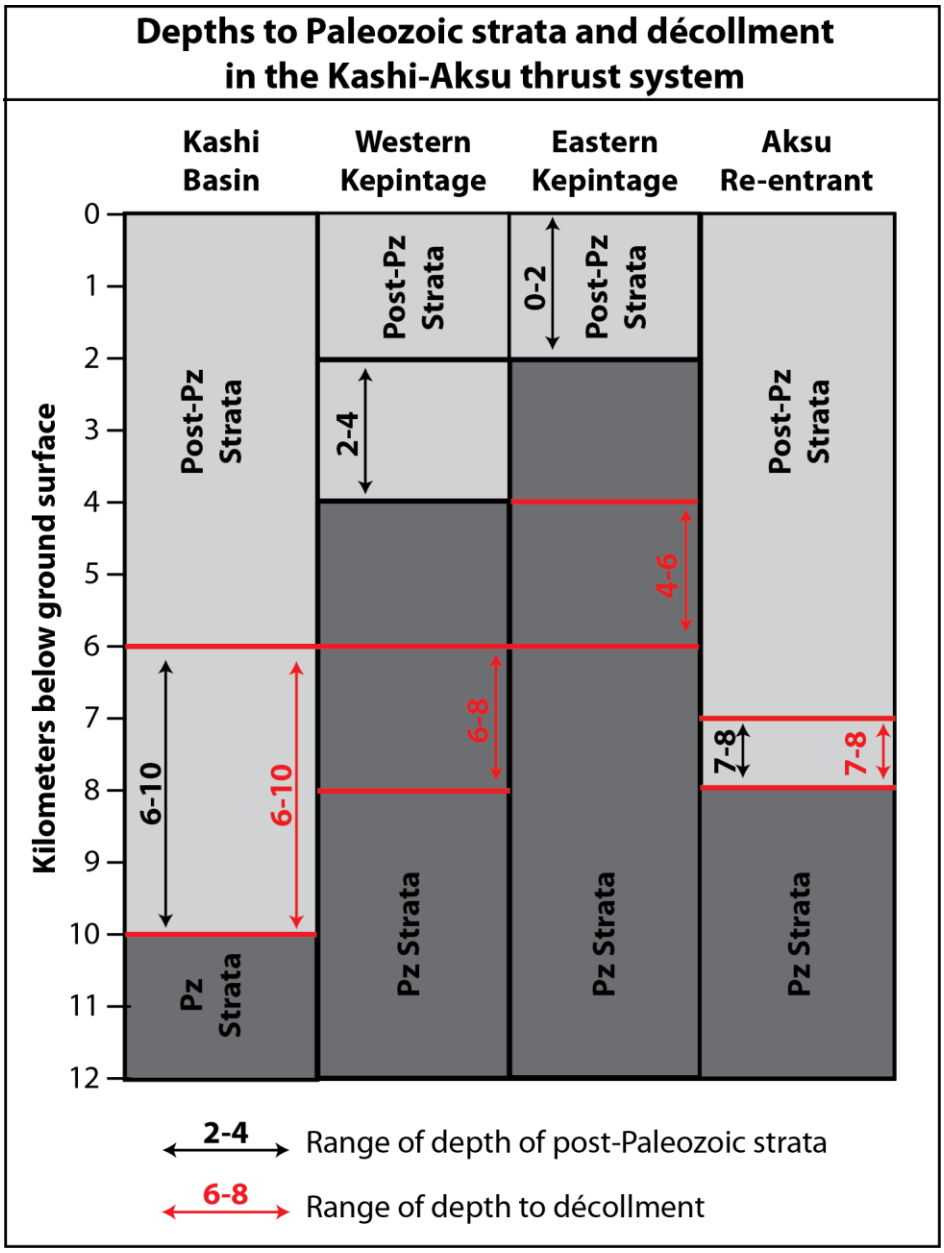

Figure 20 – Depths to Paleozoic strata and detachment horizon in the Kashi-Aksu thrust system (McKnight, 1994; Yin et al., 1998; Scharer et al., 2004; Heermance et al., 2008; and this study).

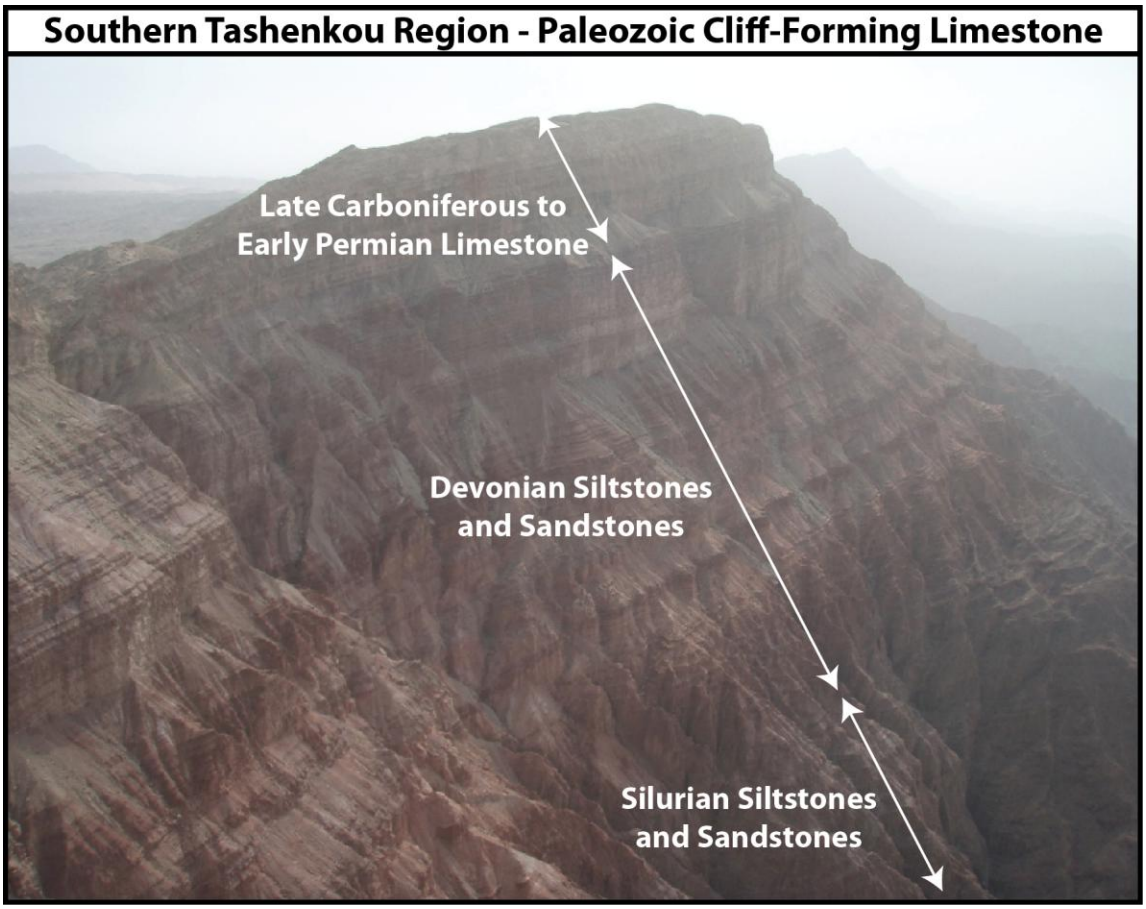

Figure 21 – Paleozoic limestone is the cliff-forming strata in the western Kepintage.

APPENDIX B: MAGNETOSTRATIGRAPHY

Methods for Magnetostratigraphy

Due to the lack of faunal and floral fossils within the sediments, as well as a lack of volcanic layers, dating of the Neogene section is done wholly through magnetostratigraphy. Core and/or block samples, for the purpose of magnetostratigraphy, were collected approximately every 5 m for the entire Neogene section. One to two samples per sample location were oriented, labeled and catalogued (samples are referred to herein as paleomagnetic samples). Each sample location was recorded with a GPS unit and logged on the stratigraphic column. Each sample was secured in a sample bag and was transported back to the United States as carry on luggage.

Samples collected in the field were cored from the rock using a hand held, gas powered, diamond bit drill (Figure A1). When sampling was unable to be completed with the drill, block samples were taken. Strike and dip of the orientation of each sample, as well as strike and dip of the bedding plane from which the sample was taken, were recorded to preserve the in situ orientation of the samples. The sample number and the orientation were labeled directly on each sample.

A sampling interval of approximately 5 m was used to maximize the likelihood of collecting multiple samples within each magnetic reversal. Sedimentation rates of Tertiary strata in the northern Tarim basin are 200-800 m/Myr (e.g.: Chen 2002, 2007; Heermance et al., 2007). The mean duration of magnetic polarity reversals, or chrons, is 300 Kyr, with chrons as short as 20 kyr (Dupont-Nivet and Krijgsman, 2012). At a sedimentation rate of 200 m/Myr, a 20 kyr interval would be represented by strata 4 m thick, and a 800 m/Myr sedimentation rate over the same interval would yield a stratigraphic thickness of 16 m. By assuming the average sedimentation rate of the region, 500 m/Myr, sampling every 5 m all but guarantees multiple sample sites within each chron.

Samples were primarily taken from fine-grained red beds. Fine-grained sediments preserve paleomagnetism better than coarse-grained sediments because single domain (all magnetism is in the same direction) particles are more stable for longer periods of time (Dupont-Nivet and Krijgsman, 2012). Beds that were red in color were also preferentially sampled, red sediments tend to have higher concentrations of hematite, or more fundamentally, ferric iron (or rust). Ferric iron records the magnetic polarity well due to its inherit magnetism. When sampling in large sections of strata that were primarily coarse (i.e: sandstone) or green (i.e.: anoxic mudstone), thin beds within these units with the preferred sampling criteria were sampled. In situations when no beds with the preferred sampling criteria present, samples were collected from the less desirable beds, as coarser grained sediments have often yielded decent paleomagnetic remnants (Dupont-Nivet and Krijgsman, 2012).

It is nontrivial to discuss the importance, or rather significance, of single site reversals in magnetostratigraphy. A single site reversal is simply a reversal that is recorded by only one sample site. Due to the occurrences of removal of the primary remnant magnetization in samples, such as from lightening strikes; or a rock that simply did not record the magnetic polarity, such as coarse grained sediment; single site reversals are not always reliable for representing a true reversal. Consequently, single

site reversals are often not used in magnetostratigraphy, or when they are used it is noted that they are not as reliable as reversals represented by several data points.

All samples collected in the field were cut at the California State University Northridge rock laboratory. Each sample was cut and/or filed to the appropriate size, approximately 2.5 cm in diameter and 2 cm long, for paleomagnetic analysis while still preserving the orientation of the rock in the field (Figure A2). Samples were then transported to the Occidental College Paleomagnetism Laboratory for analysis. Each sample was run in the Paleomagnetism Laboratory by Jeff Cook, and magnetostratigraphy correlation to the Global Paleomagnetic Time Scale (GPTS) was completed by Richard Heermance.

Magnetostratigraphy and sedimentation rates for the western Kepintage

Correlation of the measured section to the GPTS produced approximate age ranges of the Neogene strata. There is superb correlation of our data to the GPTS between stratigraphic levels 1800 m and 3400 m to the Gilbert and Gauss chrons, little is left to the imagination in this portion of the correlation. However, the paleomagnetic data is not as well behaved below 1800 m. Two correlations are presented in Figure A3, correlation alternatives A and B. Alternative B uses no single site reversals, however it produces sedimentation rates that are rather high and less likely given the known sedimentation rates in the region. Moreover, this correlation also assumes very few missed reversals, which, given the presence of a rather thick coarse-grained sandstone unit, is an assumption that may not be apposite. Alternative A uses single site reversals and presumes that several reversals were missed during sampling; this alternative produces sedimentation rates (sedimentation rates are discussed below) that are within established ranges for the region, as well as take into consideration the high possibility that reversals were missed in the thick sandstone unit.

The assumption that reversals were missed is probable; a "good" paleomag sample comes from fine grained red strata as discussed earlier in the text, this is unfortunately not what was encountered in the field at all times. The strata where reversals are presumably missed are mostly sandstones. Sandstone is typically not good for paleomag sampling, the grains are simply too coarse. We relied on inter-bedded fine-grained layers within the sandstone for paleomag sampling; otherwise, samples were taken within the sandstone in hopes that paleomagnetic polarity was imprinted. In these units, it was not uncommon for several tens of meters of section to have no interbedded fine grained layers. This increases the likelihood of missing a reversal. Therefore, it is not a leap to assume reversals were missed in the sampling. By assuming a range of sedimentation rates that falls within previously published data in this geographic region, conjecture can be made as to where these missed reversals lie in the stratigraphy, as well as which single site reversals may represent actual paleomagnetic reversals. Regardless as to whether alternative A or B is preferred, the correlation for both alternatives is the same for the sediments deposited after approximately 7 Ma. For the purposes of constraining the age of the youngest pre-deformation strata, as needed for determining shortening rates, correlation of the last 7 Ma is sufficient.

The Neogene section just below the Xiyu Conglomerate correlates to the GPTS in the Matuyama chron, more specifically, to approximately 2.1 Ma. Due to the coarse-grained nature of a conglomerate, "good" paleomag samples were difficult to obtain

within the Xiyu. Moreover, there were several single site reversals back to back in the Xiyu making determination as to whether the remnant magnetism was normal or reversed a difficult task. This can be resolved by extrapolation of sedimentation rates. Sedimentation estimates were made by plotting age versus stratigraphic height (Figure A4) for correlation alternative A. By fitting a "best-fit line" to the points, a slope of the line is determined; the slope of the line is the sedimentation rate. The best-fit line yielded a slope, or sedimentation rate, of 350 m/Ma, with a distinct increase in sedimentation rates between approximately 7.8 and 7.2 Ma. This change in sedimentation rate is within the sandstone units of the section, the grain size may be the cause of this change. An increase in sedimentation rates with larger grain sizes has been observed in quaternary loess deposits in China as in Vandenberge's (1997) study.

A sedimentation rate of 350 m/Ma is within the expected range of 200 – 800 m/Ma as discussed earlier. This places the base of the Xiyu at 1.6 Ma, and the growth strata at approximately 0.9 Ma. The age of the growth strata are used as a lower age limit for determining rates.

APPENDIX C: MAGNETOSTRATIGRAPHY FIGURES

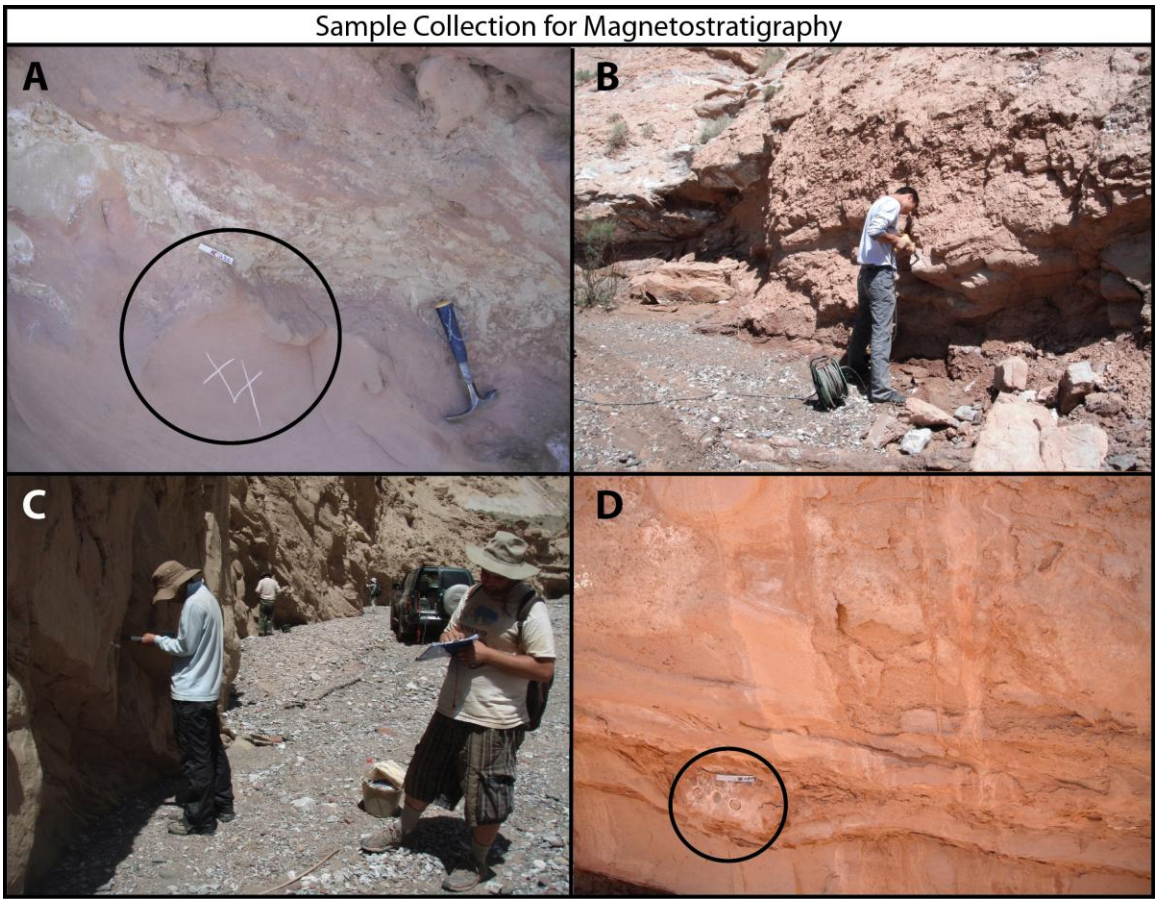

Figure A1 - Sampling for magnetostratigraphy. A) Mark location of sample on strata with X and nail ID tag to strata. B) Drill sample core from strata. C) Measure orientation of core sample in situ and record dip of strata. D) Core samples removed from strata.

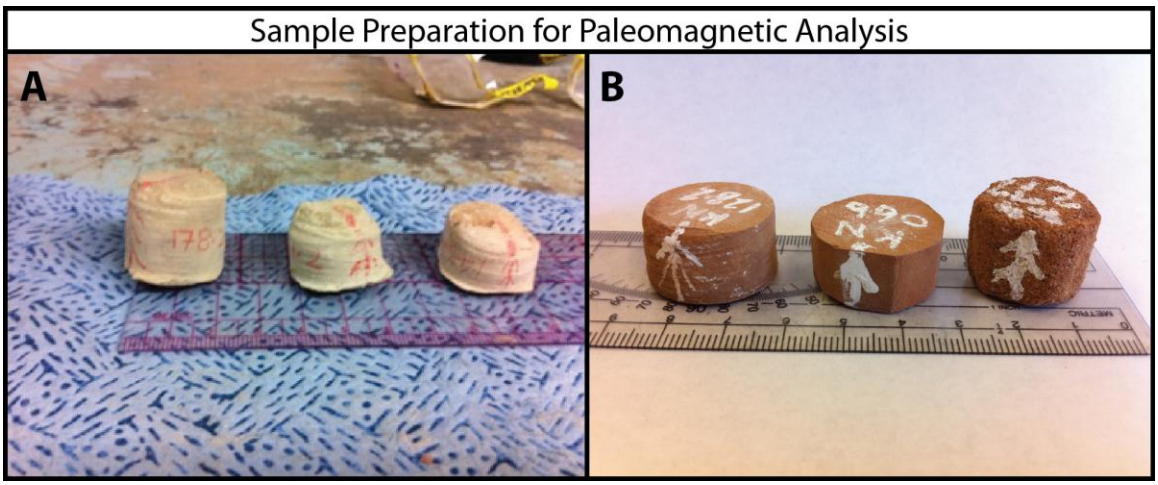

Figure A2 - Core sample preparation for paleomagnetism analysis. A) Raw samples from the field. B) Samples that have been filed to size and relabeled, ready for analysis.

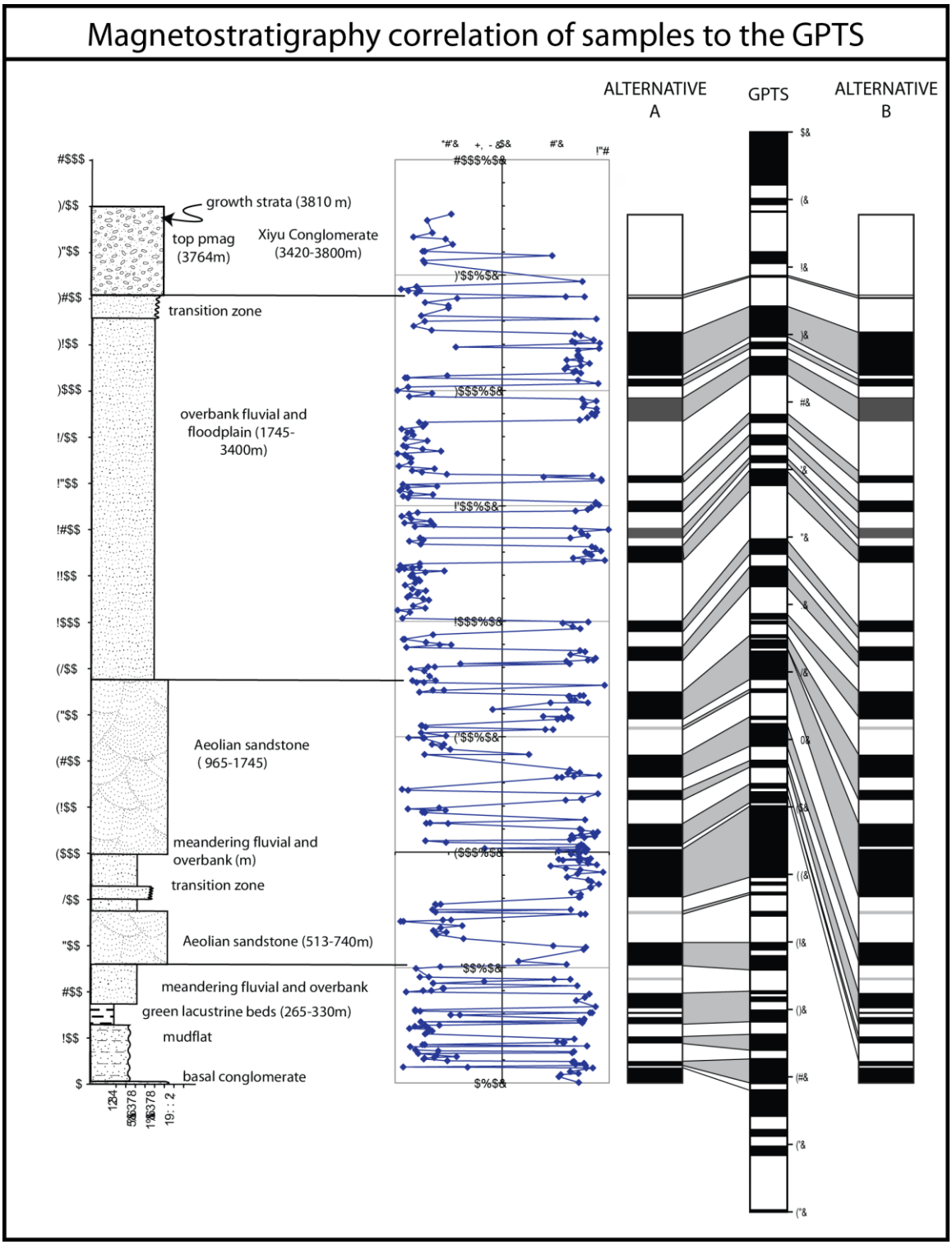

Figure A3 - Magnetostratigraphy correlation of samples to the GPTS. Alternative A and B show similar correlations above 7Ma. Alternative A is the preferred correlation and is the correlation used in determining sedimentation rates in Figure A4. Alternative B produced sedimentation rates that are unreasonably high.

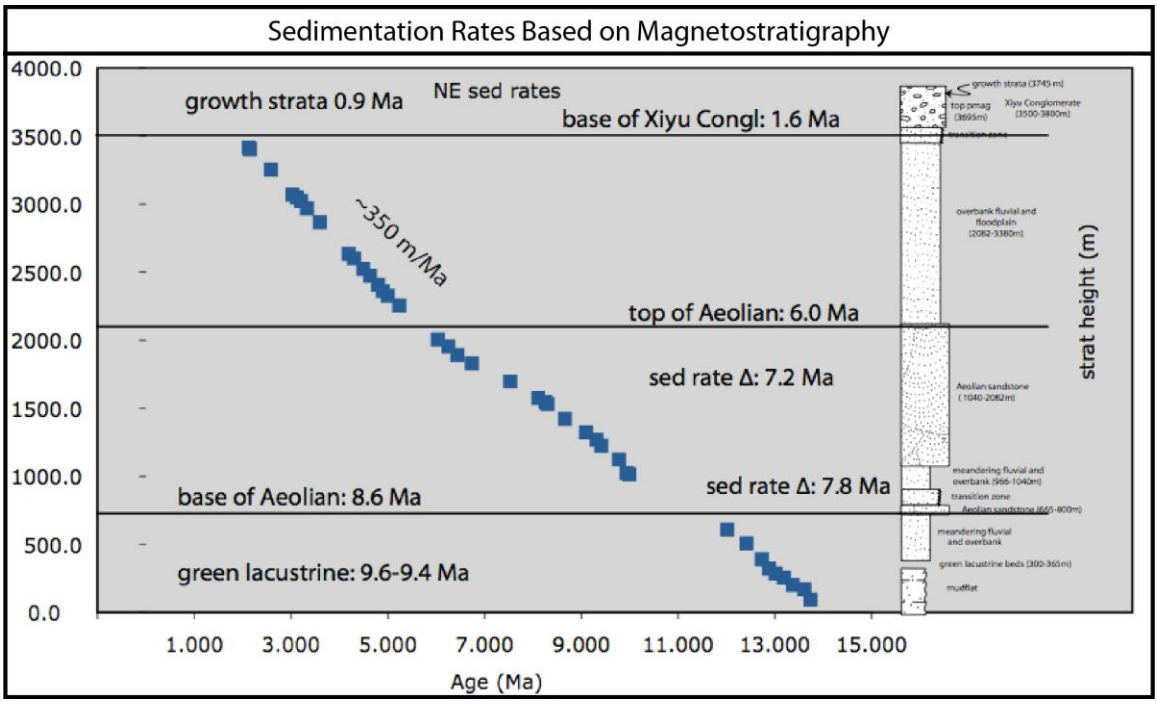

Figure A4 - Sedimentation rates using Alternative correlation A from the magnetostratigraphy. Sedimentation rates are 350 m/Ma, with an increase in sedimentation rate to 1000 m/Ma between 7.8 and 7.2 Ma.

APPENDIX D: TRISHEAR

Trishear modeling is a somewhat unexploited approach to cross section modeling, as it requires numeric modeling and the use of programs and cannot be modeled by hand as can kink-band modeling. Before discussing the actual structures of the western Kepintage, I will describe trishear modeling and how it is applied to fault studies.

Trishear was first introduced by Erslev in 1991 as a way to more accurately describe fold geometries observed in nature that cannot be explained with typical kink-band models (Erslev, 1991; Hardy and Ford, 1997; Allmendinger, 1998). Kink-band modeling cannot be used to explain changes in bedding thickness in the backlimb or forelimb of a structure, and often fails to explain curved fold hinges (e.g.: Erslev, 1991, and Cristallini and Allmendinger, 2002). Moreover, kink-band models produce uniform dips of limbs and cannot allow for changes in dip often observed in nature (Erslev, 1991). Trishear modeling can account for variable dips of bedding in the hanging wall and bedding thickness changes often observed in fold geometries. In the trishear model, the forelimb of a fault-propagation fold tightens and converges downward toward the fault tip in a triangular zone (in cross section) (Figure 6). This zone is what is referred to as the trishear zone (Erslev, 1991). Erslev (1991) explains the trishear zone as a zone that accommodates "strain-compatible shear in a triangular zone". If [in a thrust fault] the shear zone were restricted to the hanging-wall or footwall, volume would either be lost or gained, respectively (Figure 6). However, if the shear zone is evenly split between the hanging wall and footwall, no volume is gained or lost (Erslev, 1991). To maintain equal area pre- and post-deformation, material must be moved from the hanging-wall to the footwall in a direction oblique to the fault (Erslev, 1991). Fundamentally, trishear modeling allows for shear deformation, or an anisotropic component, in a traditionally wholly isotropically modeled structure.

The modeling program used for this study is FaultFoldForward (FFF), one of the few trishear programs available (Allmendinger, 2012). In order to construct a trishear model on FFF the following criteria must be entered into the modeling program:

Ramp angle – This is the dip of the fault; it can be determined by the dip of the strata exposed above the fault surface. No actual bedding dip data are input into the program.

Trishear angle – To determine trishear angle, the triangular zone of shear needs to be identified. This can be accomplished iteratively by superimposing different models over a true cross sectional view (based on field observations such as photo, sketch, or seismic imagery) of the structure.

Total slip – This is the net displacement on the fault surface. Note that with a fault-propagation fold, slip on a fault surface will decrease up dip; therefore, this does not refer to the amount of displacement that can be seen on the surface, rather the maximum displacement that is revealed at depth on the fault plane. If actual displacement on the fault is unknown, this is determined iteratively.

Propagation/Slip (P/S) ratio – This is the ratio of how far the structure has propagated, or moved, relative to how much slip has occurred on the fault surface. According to Hardy and Ford (1997) low P/S ratios (P/S<1) will result in thickening of the forelimb and tight folding within the trishear zone, while high P/S ratios (P/S>1) will exhibit less thickening and more open folding within the trishear zone. This ratio can have considerable effect on the appearance of the structure, and is determined iteratively.

Additional information is needed in order to complete the modeling including, but not limited to, unit thickness, fault type (thrust or normal), and point of initiation of faulting on an XY axis. This information, along with other modeling data, is not discussed herein since the modeling program itself is not part of the objective of this study.